Mössbauer diffraction. III. Emission of Mössbauer γ rays from crystals. B. Dynamical solutions*

J. P. Hannon, N. J. Carron†, and G. T. Trammell
Physics Department, Rice University, Houston, Texas 77001
(Received 16 August 1973)

The dynamical solutions for the emission of Mössbauer γ rays from crystals are examined. It is found that enhanced-intensity "anomalous-emission" Kossel lines occur in the early development of an active source as a consequence of the fact that the electronic scattering absorption of the lattice is predominantly $E1$, while most Mössbauer transitions correspond to the emission of higher-order-multipole waves. The sensitivity of the Mössbauer scattering to the magnetic field and electric-field-gradient tensor at the nucleus gives rise to "magnetic Kossel cones" which uniquely exhibit the structure of the internal fields when it differs from the chemical structure of the crystal. Faraday effects are also important in describing the polarization state of the emitted γ quanta. The phase of the x-ray structure factor of (molecular) crystals can be determined by Kossel-cone analysis. Applications of the theory to the problems of obtaining enhanced highly collimated Mössbauer-γ-ray sources, and the problems of magnetic and chemical structure determinations by Kossel-cone analysis are presented.

I. INTRODUCTION

In the preceding paper[1] we developed the theory for the emission of Mössbauer γ rays from single crystals. In this paper we examine the dynamical solutions for the cases of emission into Laue, Bragg, off-Bragg, and grazing-incidence channels, and give applications of the theory to the problems of obtaining enhanced collimated sources and the problems of magnetic and chemical structure determinations.

Interesting new features arise in the emission of Mössbauer γ rays from crystals. These features were discussed qualitatively in the introduction to paper IIIA. The present paper gives the first treatment of the anomalous-emission effect, the magnetic Kossel effect, the Faraday effect in emission, and the first discussion of the possible use of Kossel-line analysis to determine the phase of the unit-cell structure factor.

In Sec. II we consider emission into Laue channels. We discuss in particular the anomalous-emission effect and its application to the problem of obtaining enhanced collimated sources, the magnetic Kossel effect, and the frequency spectrum of Kossel lines from Zeeman-split sources. In Sec. III we treat emission into Bragg channels and discuss the problem of phase determination by Kossel-line analysis. In Sec. IV we consider off-Bragg emission and the related Faraday effects, and finally in Sec. V we treat emission into grazing-incidence channels.

II. LAUE CHANNELS

The most striking feature in the single-crystal x-ray or Mössbauer emission pattern is the Kossel-line structure. If $\vec{R}$ denotes an observation point sufficiently far from the source, then the Kossel lines occur for $\vec{k} = (\omega/c)\hat{R}$ satisfying a Bragg condition with some set of crystal planes. These lines are observed on a photographic plate as conic sections which have an intensity somewhat greater or less than background intensity and, under high resolution, have a dark-light fine structure. There will be two different types of Kossel lines, for $\vec{k}$ corresponding to a Laue (or Borrmann) transmission channel (Laue case) and for $\vec{k}$ corresponding to a Bragg-reflection channel (Bragg case). We shall consider the latter in Sec. III.

Explicitly the radiation field above the top layer of the crystal is given by Eq. (62) of IIIA:

$$\vec{A}_M(\vec{R}) = \int_> \vec{A}_M(\vec{k}) \exp[i\vec{k}\cdot(\vec{R} - z_M\hat{z})]\, d\Omega_k\,, \quad z > z_M\,.$$

For large R, from Eq. (90) of IIIA,

$$\vec{A}_M(\vec{R}) \sim \frac{2\pi}{ik}\vec{A}_M(\vec{k})\frac{\exp(ik|\vec{R} - z_M\hat{z}|)}{|\vec{R} - z_M\hat{z}|}\,,$$

with $\vec{k} = k\hat{R}$, so that the direction of observation $\hat{R}$ determines the "channel" $\vec{k} = k\hat{R}$ at the top of the crystal which contributes to $A_M(\vec{R})$. Unless $\vec{k}$ is near a Bragg angle for some crystal planes

$$\vec{A}_M(\vec{k}) = \tilde{D}_j^M(\vec{k}, \vec{k})\vec{J}_\perp(-\vec{k}, \omega; j) \text{ (off Bragg)}$$

and channel $\vec{k}$ at the top of the crystal is "fed" only by the waves emitted into the channel $\vec{k}$ by the emitting atom at $\vec{R}_j$. For these directions $\tilde{D}_j^M(\vec{k}, \vec{k})$ is a slowly varying function of $\hat{k}$, merely representing the transmission of the coherent wave through the crystal without scattering.

If $\vec{k}$ is near a Bragg angle for the Laue case, then with $\vec{k}_1(\vec{k})$ given by Eq. (61) of IIIA,

$$\vec{k}_1 = [k^2 - (\vec{k}_{xy} - \vec{\tau}_1)^2]^{1/2}\hat{z} + \vec{k}_{xy} - \vec{\tau}_1\,. \tag{1}$$

where $\vec{\tau}_1$ is some *planar* reciprocal-lattice vector, the near- Laue condition is given by [Eq. (60b) of IIIA]

$$(g-g_1)d = 2\pi m + 2\delta, \tag{2}$$

where $g \equiv k_z = (k^2 - \vec{k}_{xy}^2)^{1/2}$, and δ is small ($\delta = 0$ is the exact Bragg condition). If (1) and (2) are satisfied we say that $\vec{k}$ and $\vec{k}_1$ are Laue (transmission) channels. In this case we have [Eq. (66) of IIIA]

$$\vec{A}_M(k) = \tilde{D}_j^M(\vec{k}, \vec{k})\vec{J}_\perp(-\vec{k}, \omega; j) + \tilde{D}_j^M(\vec{k}, \vec{k}_1)\vec{J}_\perp(-\vec{k}_1, \omega; j), \text{ (Laue)} \tag{3}$$

and channel $\vec{k}$ at the top of the crystal is "fed" coherently by both the waves emitted by the atom at $\vec{R}_j$ into channel $\vec{k}$ and into channel $\vec{k}_1$. For $\vec{k}$ in the vicinity of a Laue channel, $\tilde{D}(\vec{k},\vec{k})$ and $\tilde{D}(\vec{k},\vec{k}_1)$ are very rapidly varying functions of $\hat{k}$ and give rise to the appearance of the (Laue) Kossel cones in these directions.

If we reverse the sign of g_1 so that $k_{1z} < 0$, in Eqs. (1)–(3), we have the conditions for the Bragg case, the corresponding $\vec{k}$ and $\vec{k}_1$ being "Bragg-reflection channels," which we discuss in detail in Sec. III.

In Fig. 1 we indicate the two channels at the emitting atom, located at $\vec{R}_j$ in the mth layer, feeding the $\vec{k}$ channel at the top surface (Mth layer). The channels $\vec{k}$ and $\vec{k}_1$ are Bragg reflected into each other by the crystal planes indicated in the figure.

δ in Eq. (3) is given in terms of the deviation $\Delta\varphi = (\varphi - \varphi^B)$ of the rocking angle φ from the exact Bragg angle ϕ^B by, $\delta = (kd\sin\theta)\Delta\varphi/2\sin\varphi_1$, where θ is the scattering angle (Fig. 1).

The coherent wave propagator matrices $\tilde{D}_j^M$ can [Eq. (76) in IIIA] be expressed in terms of the $\tilde{\mathcal{T}}$ matrices, $\tilde{\mathcal{T}}_{M-m}(\vec{k}, \vec{k})$ and $\tilde{\mathcal{T}}_{M-m}(\vec{k}, \vec{k}_1)$, which were defined in Eqs. (71) and (72) of IIIA. With the aid of Eq. (76) of IIIA we may rewrite Eq. (3) in the form

$$\vec{A}_M(\vec{k}) = \frac{ik}{2\pi}\left(\tilde{\mathcal{T}}_{M_j}(\vec{k}, \vec{k})e^{-i\vec{k}\cdot\vec{\rho}_j}\vec{J}_\perp(-\vec{k}, \omega; j) + \tilde{\mathcal{T}}_{M_j}(\vec{k}, \vec{k}_1)\frac{\sin\phi}{\sin\phi_1}e^{-i\vec{k}_1\cdot\vec{\rho}_j}\vec{J}_\perp(-\vec{k}_1, \omega; j)\right), \tag{4}$$

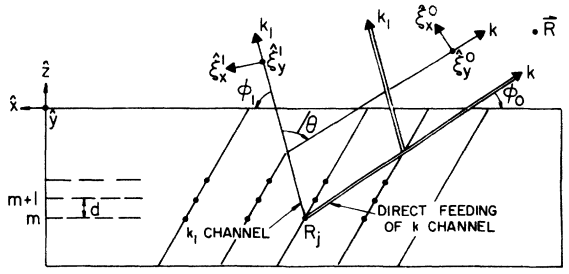

FIG. 1. Schematic representation of a Laue emission channel. The wave fed directly into the k channel by the source is indicated by the double line, and the wave reflected into the k channel from the k_1 channel which interferes with the direct wave is indicated by the single line.

where $M_j = M - m_j + 1$ is the number of layers below the surface where the emitter is located, and $\vec{\rho}_j = \vec{r}_j - \vec{R}_{mj}$ is the position of the emitter taking the origin as the lattice point of the unit cell in which the emitter is located.

The $\tilde{\mathcal{T}}_{M_j}(\vec{k}, \vec{k})$ and $\tilde{\mathcal{T}}_{M_j}(\vec{k}, \vec{k}_1)$ give the amplitude in channel $\vec{k}$ at the top of the crystal for unit amplitude wave incident at the layer m_j in channels $\vec{k}$ and $\vec{k}_1$, respectively, and the remaining factors give the amplitudes (complex amplitude, including phases) with which the two channels are fed by the emitter at $\vec{\rho}_j$.

A general procedure for obtaining the $\tilde{\mathcal{T}}$ matrices was given in Sec. III of II.[2] In the general case of strong polarization mixing[2] numerical procedures must be resorted to. However, there are three important cases in which there is no "polarization mixing" and simple analytical expressions may be obtained.

The first two of these cases are[2] (i) no Zeeman splitting and (ii) Zeeman splitting, but the quantization axis (direction of the internal magnetic field and symmetry axis of the quadrupole field) at each Mössbauer nucleus is perpendicular to the scattering plane ($\vec{k}$, $\vec{k}_1$). Case (ii) can hold, of course, only for two points on a given Kossel cone.

If in these two cases we choose the polarization basis vectors for each of the two channels as shown in Fig. 1 with the $\hat{\epsilon}_x$'s in the scattering plane and perpendicular to their respective $\vec{k}$'s, and the $\hat{\epsilon}_y$'s perpendicular to the scattering plane, then $(\tilde{\mathcal{T}})_{xy} = (\tilde{\mathcal{T}})_{yx} = 0$.

The third case is that of a ferromagnet with strong Zeeman splitting (so that the interference of the different resonances can be neglected).[3] The concentration of the resonant scatterers is large enough that the electronic scattering absorption is negligible, and finally the nuclear transition is a pure $(L\lambda)$ multipole. In this case there is no polarization mixing if we choose as polarization basis vectors for a given channel $\vec{k}$, $\hat{\epsilon}_{LM\lambda}(\vec{k}) = \vec{Y}_{LM}^{(\lambda)}(\vec{k})/|Y_{LM}^{(\lambda)}(\vec{k})|$, and a second $\hat{\epsilon}_{LM\lambda}^{\perp}(\hat{k})$ perpendicular to it. An $\hat{\epsilon}_{LM\lambda}^{\perp}(\hat{k})$ polarized photon in fact will not scatter or be absorbed, and so in this third case it is only the $\hat{\epsilon}_{LM\lambda}(\hat{k})$ polarization which is relevant. $\vec{Y}_{LM}^{(\lambda)}(\hat{k})$ is the vector spherical harmonic for the $LM\lambda$ transition and is given explicitly by Eqs. (A2)–(A2″) for $E1$ ($L=1$, $\lambda=1$), $E2$ ($L=2$, $\lambda=1$), and $M1$ ($L=1$, $\lambda=0$) transitions.

Now in the case of no polarization mixing [cases (i)–(iii) with the choice of polarization basis vectors indicated above] the $\tilde{\mathcal{T}}$ and $\tilde{D}$ matrices are diagonal, and $(\tilde{\mathcal{T}}(\vec{k}, \vec{k}_1))_{\lambda\lambda}$ and $(\tilde{\mathcal{T}}(\vec{k}, \vec{k}))_{\lambda\lambda}$ are given by Eqs. (53) and (54) of II, respectively. We have

$$(\tilde{\mathcal{T}}_{M_j}(\vec{k}, \vec{k}))_{\lambda\lambda} = [\cos M_j\beta_\lambda + i\nu_\lambda(\sin M_j\beta_\lambda)/\beta_\lambda] \times \exp[iM_j(\alpha_\lambda + gd - \delta)] \tag{5a}$$

and

$$(\vec{\mathcal{T}}_{M_j}(\vec{k}, \vec{k}_1))_{\lambda\lambda} = iF_{\lambda\lambda}(\vec{k}, \vec{k}_1)[\sin M_j\beta_\lambda)/\beta_\lambda] \times \exp[iM_j(\alpha_\lambda + gd - \delta)]. \quad (5b)$$

Here $\lambda = x$ or y, or for the ferromagnetic case $\lambda = LM\lambda$ corresponding to the $\hat{\epsilon}_{LM\lambda}$ polarization. $M_j = M - m_j$ is the number of layers below the surface at which the decay occurs. The remaining terms are given by

$$\nu_\lambda = \delta + \tfrac{1}{2}[F_{\lambda\lambda}(\vec{k}, \vec{k}) - F_{\lambda\lambda}(\vec{k}_1, \vec{k}_1)], \quad (6a)$$

$$\alpha_\lambda = \tfrac{1}{2}[F_{\lambda\lambda}(\vec{k}, \vec{k}) + F_{\lambda\lambda}(\vec{k}_1, \vec{k}_1)], \quad (6b)$$

$$\beta_\lambda = [\nu_\lambda^2 + F_{\lambda\lambda}(\vec{k}, \vec{k}_1)F_{\lambda\lambda}(\vec{k}_1, \vec{k})]^{1/2}, \quad \mathrm{Im}\,\beta_\lambda > 0. \quad (6c)$$

δ is given by (2) and the planar scattering amplitudes are given by

$$F_{\lambda\lambda'}(\vec{k}_a, \vec{k}_b) = \frac{n\lambda d}{\sin\phi_a} \sum_\rho f^{(\rho)}(\hat{\epsilon}_\lambda(\vec{k}_a), \vec{k}_a; \hat{\epsilon}_{\lambda'}(\vec{k}_b), \vec{k}_b) \times e^{-i(\vec{k}_a - \vec{k}_b)\cdot\vec{\rho}}, \quad (7)$$

where n is the density of unit cells (cm^{-3}), the sum is over the unit cell, $\vec{\rho}$ is the position of an atom in the unit cell relative to the Bravais lattice point in that unit cell, and $f^{(\rho)}$ is the elastic coherent scattering amplitude for the atom at $\vec{\rho}$ [the sum in (7) is simply the unit-cell structure factor].

Since the Jacobian $|d\Omega_{k_1}/d\Omega_k| = \sin\phi/\sin\varphi_1$ always enters as a factor multiplying the "cross channel" terms, e.g., $\tilde{\mathcal{T}}(\vec{k}, \vec{k}_1)$ in (4) or $\tilde{\mathcal{R}}(\vec{k}, \vec{k}_1)$ in Eq. (82) of IIIA, it is convenient to include this factor in the definition of the $\tilde{\mathcal{T}}$ and $\tilde{\mathcal{R}}$ matrices. Similarly, the factor $ik/2\pi$ in (4) and in Eq. (82) of IIIA is conveniently absorbed in the definition of $\vec{A}$. In fact we see from Eq. (90) of IIIA that $A'_M(\vec{k})$ in (8a) is the amplitude of the emitted wave at large distances from the emitter. We define

$$\vec{A}'_M(\vec{k}) = (2\pi/ik)\vec{A}_M(\vec{k}), \quad (8a)$$

$$\tilde{\mathcal{T}}'_m(\vec{k}_a, \vec{k}_b) = (\sin\phi_a/\sin\phi_b)\,\tilde{\mathcal{T}}_m(\vec{k}_a, \vec{k}_b), \quad (8b)$$

$$\tilde{\mathcal{R}}'_m(\vec{k}_a, \vec{k}_b) = (\sin\phi_a/\sin\phi_b)\tilde{\mathcal{R}}_m(\vec{k}_a, \vec{k}_b), \quad (8c)$$

$$\tilde{F}'(\vec{k}_a, \vec{k}_b) = (\sin\phi_a/\sin\phi_b)\,\tilde{F}(\vec{k}_a, \vec{k}_b). \quad (8d)$$

With these substitutions (4) now takes the form

$$\vec{A}'_M(\vec{k}) = \tilde{\mathcal{T}}'_{M_j}(\vec{k}, \vec{k})\, e^{-i\vec{k}\cdot\vec{\rho}_j}\vec{J}_\perp(-\vec{k}, \omega; j) + \tilde{\mathcal{T}}'_{M_j}(\vec{k}, \vec{k}_1)e^{-i\vec{k}_1\cdot\vec{\rho}_j}\vec{J}_\perp(-\vec{k}_1, \omega; j). \quad (4')$$

It is easily seen that $\tilde{\mathcal{T}}'$ and $\tilde{\mathcal{R}}'$ are the same function of $\tilde{F}'$ as $\tilde{\mathcal{T}}$ and $\tilde{\mathcal{R}}$ are of $\tilde{F}$ $\{\alpha_\lambda, \beta_\lambda, \nu_\lambda$ [Eq. (6)] are invariant under $\tilde{F} \to \tilde{F}'\}$.

Finally the transition currents in (4) or (4′) are given by Eq. (15) of IIIA for a radioactive decay or by Eqs. (29) or (39) of IIIA for currents resulting from incoherent scattering. The explicit form of these currents for $E1$, $M1$, and $E2$ transitions are given by Eqs. (A1) – (A2″).

Hereafter, for brevity we will call the $\vec{k}$ channel the 0 channel and the k_1 channel the 1 channel, and shall write $F'(\vec{k}, \vec{k}_1)$ as F^{01}, $\hat{\epsilon}_\lambda(\vec{k})$ as $\hat{\epsilon}^0_\lambda$, etc.

If the emitter is deep in the crystal, i.e., M_j is greater than the off-Bragg extinction depth $(\mathrm{Im}\alpha_\lambda)^{-1}$, then the dominant contribution to (4′) comes from the exponential terms depending on the difference between α_λ and β_λ. Thus for the source deep in the crystal, the wave emitted from the crystal in a Laue channel is

$$\vec{A}'_M(\vec{k}) = \sum_{\lambda=x,y} \hat{\epsilon}^{(0)}_\lambda K_\lambda(\delta, \omega; R_j)e^{iM_j(\alpha_\lambda - \beta_\lambda)}, \quad (9)$$

where

$$K_\lambda = \tfrac{1}{2}[e^{-i\vec{k}\cdot\vec{\rho}_j}\hat{\epsilon}^{(0)}_\lambda \cdot \vec{J}^{f0}_\perp(-\vec{k}, \omega; j)(1 - \nu_\lambda/\beta_\lambda) - e^{-i\vec{k}_1\cdot\vec{\rho}_j}\hat{\epsilon}^{(1)}_\lambda \cdot \vec{J}^{f0}_\perp(-\vec{k}\ \omega; j)(F^{01}_{\lambda\lambda}/\beta_\lambda)]. \quad (10)$$

The exponential factor in (9) determines the penetration depth $l_\lambda(\delta)$ of the Laue channel emission,

$$l_\lambda(\delta) = d[\mathrm{Im}(\alpha_\lambda - \beta_\lambda)]^{-1}. \quad (11)$$

If a source is located within a depth l_λ from the surface, radiation will be emitted from the crystal in a Laue channel *unless* the interference term K_λ is destructive, as is the case for x-ray optics. The penetration depth is, in general, different for the two polarizations $\hat{\epsilon}^0_x$ and $\hat{\epsilon}^0_y$. Initially the penetration depth is that of the x-ray "Borrmann case." For a developed source, the Laue penetration depth for the *recoilless* fraction depends strongly on the concentration and multipolarity of the resonant scatterers.

The factor K_λ in (9) gives the interference of the waves in the k channel which are set up by the source coherently feeding the k and k_1 channels, as indicated schematically in Fig. 1. Depending on the multipolarity of the source and the location of the source, e.g., regular *lattice site* or *interstitial*, the interference term can be constructive, in which case the emission is enhanced, or destructive, so that the emission is suppressed.

A. Anomalous emission effect

The phenomena of crystal emission into von Laue channels arising from sources located at lattice sites deep within the crystal is peculiar to Mössbauer emission. In contrast such emission is strongly suppressed in x-ray optics. We shall see that such emission occurs for both the recoilless and recoil fractions from Mössbauer sources of multipolarity $M1$ or higher in the "early development" of the source crystal when the concentration of resonant scatterers is small, and that the emitted radiation is linearly polarized everywhere tangent to the Kossel cone. We will refer to this effect as the "anomalous-emission effect."

The anomalous-emission effect is closely related

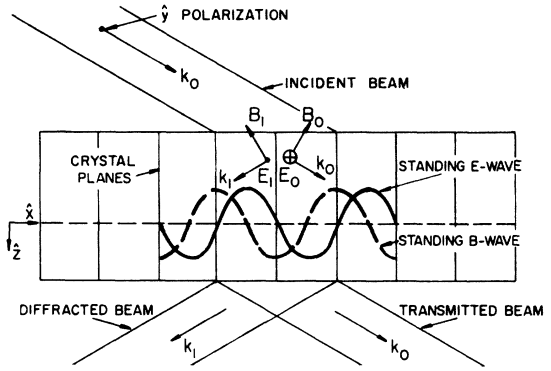

FIG. 2. Schematic representation of the x-ray Borrmann effect. The solid wavy line represents the standing E wave with nodes at the crystal planes. The dotted wavy line represents the standing B wave (or electric field gradient) with antinodes at the crystal planes.

to the Borrmann effect[4] of x-ray optics, indicated schematically in Fig. 2. The Borrmann effect shows that radiation incident near a Bragg angle on a set of Laue planes of an absorbing crystal may have orders-of-magnitude-greater penetration depth than that incident at ordinary angles. This occurs because the two diffracting waves set up a standing-wave pattern with nodes at the atomic planes which leads to a suppression of atomic absorption processes and hence to much deeper penetration of the radiation within the crystal.

Similarly a photon emitted from within a crystal in a direction satisfying the Bragg condition for a set of Laue planes will propagate much farther than one emitted in an ordinary direction. We might then expect that a thick perfect crystal doped with active Mössbauer isotopes could serve as a highly enhanced source of very-well-collimated Mössbauer γ rays.

In x-ray optics no such phenomenon is observed, and in fact the Kossel lines are characterized as much by a minimum in intensity as by a weak maximum. This limitation to the brightness gain in the Kossel cones for x-ray emission stems from the fact that the two interfering waves which are responsible for the anomalous Borrmann transmission through a thick crystal are each fed by the spherical outgoing $E1$ wave from the source with relative phases such as to cancel the transmitted waves (shown schematically in Fig. 1). This result also appears from the use of the von Laue reciprocity theorem, which for x-ray optics, where one has $E1$ sources and scatterers, may be stated as follows[5,6]: "If a source of radiation and a point of observation are interchanged, the intensity, measured in terms of the electric displacement, is the same at the new place of observation as at the old." Now in the anomalous transmission of a wave incident from outside the crystal, there is near cancellation of the electric field at the regular lattice sites deep in the crystal; but by the reciprocity theorem this implies that an $E1$ wave emitted from such a site will not be emitted from the crystal.

On the other hand for Mössbauer-γ-ray optics anomalous emission will occur in the early development of a crystal containing Mössbauer emitters of multipolarity $M1$ or higher: The two Borrmann waves are fed constructively by such emitters, or from the standpoint of reciprocity [generalized as in Eq. (51) of IIIA to account for the higher-order multipolairty], while the electric field vanishes at lattice points in Borrmann transmission, the magnetic field and electric field gradient do not, as indicated in Fig. 2, so that there will be strong coupling to an $M1$ or $E2$ oscillator located at such a site. Therefore, according to the reciprocity relation [Eq. (51) of IIIA to account for the higher-order emission from an $M1$ or $E2$ source located at a lattice site deep in the crystal.

The linear polarization of the anomalous emission results because it is only the "good" $\hat{\epsilon}_y$ polarization which lies parallel to the Bragg planes (and hence to the Kossel cones) which is able to establish a Borrmann effect, i.e., to establish nodes at the lattice sites.

Explicitly, in the "early development" of the source the fraction $P(t)$ of resonant scatterers is sufficiently small that the electronic scattering absorption processes dominate the nuclear scattering absorption processes and hence during this period the penetration depth $l_\lambda(\delta)$ and the interference K_λ are determined almost entirely by the electronic processes. The maximum penetration depth is then the Borrmann depth,

$$l_y(\delta=0)=\frac{2\cos(\theta/2)}{n\sigma_e}\left(\frac{1}{1-f_D(\theta)}\right),$$
$$l_x(\delta=0)=\frac{2\cos(\theta/2)}{n\sigma_e}\left(\frac{1}{1-\cos(\theta)f_D(\theta)}\right). \tag{12}$$

Here θ is the scattering angle as indicated in Fig. 1, $f_D(\theta)$ is the Debye factor, σ_e is the total absorption cross section, and n is the unit-cell density. We have assumed that the Bragg scattering planes contain only one atom from each unit cell, and for simplicity we have assumed a symmetric Laue channel for which the scattering planes are perpendicular to the crystal surface. For the "good" $\hat{\epsilon}_y$ polarization which lies parallel to the Bragg planes and is able to establish nodes at the lattice sites, the maximum penetration is greatly enhanced over the off-Bragg penetration depth,

$$l_{0B}(\theta)=2\cos(\theta/2)/n\sigma_e, \tag{13}$$

the enhancement being

$$l_y/l_{0B} = [1 - f_D(\theta)]^{-1} \approx \frac{1}{2\sin^2(\theta/2)} \frac{\chi^2}{\langle x^2 \rangle}$$

$$= \frac{1}{2m^2\pi^2} \frac{d_B^2}{\langle x^2 \rangle}, \qquad (14)$$

where x is the displacement of an atom from its equilibrium position due to zero point and thermal motion, and where in the second line we have used the Bragg condition $k\sin\theta = m\pi/d_B$, where d_B is the interplanar distance for the particular set of Bragg planes. For the ϵ_x polarization, the enhancement is

$$l_x/l_{0B} = [1 - \cos\theta f_D(\theta)]^{-1} \approx [2\sin^2(\theta/2)]^{-1}. \qquad (15)$$

For an iron lattice at liquid-He temperature, and $\theta = 20°$, the l_y enhancement is $\approx 2.2\times10^2$, and the l_x enhancement is ≈ 17.

Of course as we have already noted, the question of whether the radiation emitted from an atom lying deep in the crystal [within a depth $l_\lambda(\delta)$ of the surface] emerges from the crystal depends upon the interference term K_λ, which depends on the nature of the source current. The expressions for the transition currents $J^{f0}(-\vec{k}, \omega; j)$ for $E1$, $M1$, and $E2$ are summarized in the Appendix.

For a *symmetric* Laue channel, the interference term at exact Bragg ($\delta = 0$) is

$$K_\lambda(\delta = 0) = \tfrac{1}{2}(1 - S_\lambda) e^{-i\vec{k}\cdot\vec{\rho}_j} \hat{\epsilon}_\lambda^{(0)} \cdot \vec{J}^{f0}(-\vec{k}, \omega; j), \qquad (16)$$

where

$$S_\lambda = e^{-i(\vec{k}_1 - \vec{k})\cdot\vec{\rho}_j} \left(\frac{F^{01}}{\beta_\lambda}\right) \frac{\hat{\epsilon}_\lambda^{(1)} \cdot \vec{J}^{f0}(-\vec{k}_1, \omega; j)}{\hat{\epsilon}_\lambda^{(0)} \cdot \vec{J}^{f0}(-\vec{k}, \omega; j)}. \qquad (17)$$

For a *lattice-site* emitter, the Bragg condition gives $\exp[i(\vec{k}_1 - \vec{k})\cdot\vec{\rho}_j] = +1$. Assuming the scattering planes only contain one atom from each unit cell, the factor $F^{01}_{\lambda\lambda}/\beta_\lambda(\delta = 0) = F^{01}_{\lambda\lambda}/[F^{01}_{\lambda\lambda}F^{10}_{\lambda\lambda}]^{1/2} = \pm 1$, the sign depending on the multipole nature of the scattering medium (the sign arises because β_λ is taken with positive imaginary part). In the early development of the crystal, when the scattering is predominantly nonresonant isotropic $E1$ scattering, $F^{01}_{\lambda\lambda}/\beta_\lambda = +1$ for $\lambda = x$ or y (for scattering angles $\theta < \pi/2$). As the source develops, the sign may change when the nuclear absorption dominates the photoelectric absorption. In this limit the sign depends on the polarization, the multipolarity of the scatterers, and if the resonant scatterers have Zeeman splitting, then there is a dependence on the specific Zeeman transition involved (i.e., upon M) and upon the orientation of the quantization axis with respect to the scattering planes. Here we will restrict our attention to the early development ($F^{01}_{\lambda\lambda}/\beta_\lambda = +1$). We will consider developed sources in a later section.

With $\exp[i(\vec{k}_1 - \vec{k})\cdot\vec{\rho}_j]$ and $F^{01}_{\lambda\lambda}/\beta_\lambda$ both given by $+1$ the nature of the interference is now determined by

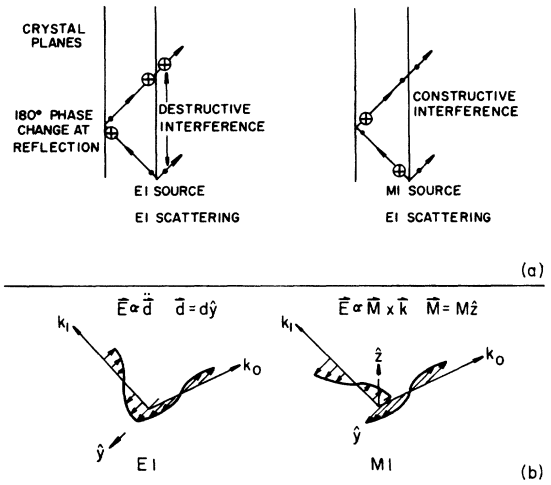

FIG. 3. (a) Schematic representation of the interference between the direct and reflected waves for $E1$ and $M1$ sources with $E1$ scattering from the lattice. (b) gives a "snapshot" of the E waves being fed into the k and k_1 channels by a linear $E1$ oscillator (i.e., a $\Delta M = 0$ transition) which oscillates along the $\hat{y}$ axis, and a linear $M1$ oscillator which oscillates along the $\hat{z}$ axis. Both send out ϵ_y polarized E fields.

the relative phase and magnitude of the source feeding of the two channels, $\hat{\epsilon}_\lambda^{(0)} \cdot \vec{J}(-\vec{k}_0)$ and $\hat{\epsilon}_\lambda^{(1)} \cdot \vec{J}(-\vec{k}_1)$. If there is no Zeeman splitting of the source, then the magnitudes are equal. In this case if the source source current feeds both channels "in phase," i.e., both with $+\hat{\epsilon}_\lambda$ polarization, then $\hat{\epsilon}_\lambda^{(1)} \cdot \vec{J}(-\vec{k}_1)/\hat{\epsilon}_\lambda^{0} \cdot \vec{J}(-\vec{k}) = +1$, so that $S_\lambda = +1$, $K_\lambda = 0$, and the interference is destructive. On the other hand, if the channels are fed "out of phase," i.e., one with $+\hat{\epsilon}_\lambda$ polarization and the other with $-\hat{\epsilon}_\lambda$ polarization, then $S_\lambda = -1$, $K_\lambda = 1$, and the interference is constructive. This is shown schematically in Fig. 3(a). The behavior of $K_\lambda(\delta)$ as a function of δ for "in phase" ($|K_-|^2$) and "out of phase" ($|K_+|^2$) feeding is shown in Fig. 4. (It should be kept in mind that if $\exp[i(\vec{k}_1 - \vec{k})\cdot\vec{\rho}_j]F'_{\lambda\lambda}/\beta_\lambda = -1$, which, as we discuss in later sections, can happen if the source is at an interstitial or as the source develops, then the roles of "in-phase" and "out-of-phase" feeding with respect to producing constructive or destructive interference are reversed.)

If there is no Zeeman splitting of the source the quantization axis $\hat{z}'$ can be chosen arbitrarily. For an $E1$ source it is convenient to take $\hat{z}'$ parallel to $\hat{\epsilon}_y$, as shown in Fig. 3(b), while for an $M1$ source we take $\hat{z}'$ in the crystal plane and perpendicular to $\hat{\epsilon}_\lambda$ as shown in Fig. 3(b). With this choice of $\hat{z}'$, the $M = 0$ transitions radiate the "good" $\hat{\epsilon}_y$ polarized radiation into the $\vec{k}$ and $\vec{k}_1$ channels (of course for the $M1$ transition there will also be an $\hat{\epsilon}_y$ component for the $M = \pm 1$ transitions, but the "feeding" of the channels is "in phase" for these transitions).

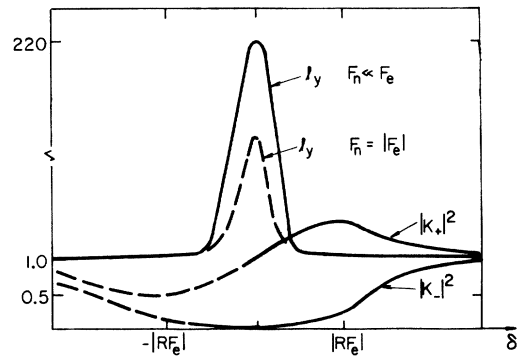

FIG. 4. Plots of the interference term $|K|^2$ and the penetration depth $l_y(\delta)/l_{0B}$ as a function of the deviation δ from exact Bragg condition for a Laue channel. The K_+ (K_-) curve is for constructive (destructive) interference between the direct and reflected waves.

For an $E1$ source, the $M=0$ transition feeds the $\vec{k}$ and $\vec{k}_1$ channels "in phase," i.e., both with $+\hat{\epsilon}_y$ radiation. As shown schematically in Fig. 3(a), the $\vec{k}$ wave reflected from the $\vec{k}_1$ channel then interferes destructively with that resulting from the "direct feeding" of the $\vec{k}$ channel. Explicitly this destructive interference of the Kossel interference term for an $E1$ transition is seen by substituting expressions (A2), into (16), which gives

$$K_y(\delta=0)=0 \quad (E1,\ M=0). \tag{18}$$

The $M=\pm1$ $E1$ transitions give ϵ_x radiation, and here there is a constructively interfering component,

$$K_x(\delta=0)=K'(\pm1)\sin(\theta/2) \quad (E1,\ M=\pm1), \tag{19}$$

where

$$K'(\pm1)=\mp\frac{3}{16\pi}C(J_0\,1\,J_n;\ m_n\pm1)\langle x_f|e^{-i\vec{k}\cdot\vec{r}}|x_0\rangle \times(\lambda\Gamma_\gamma)^{1/2}[\omega-(E_m+\epsilon_0)+(E_0+\epsilon_f)+\tfrac{1}{2}i\Gamma]^{-1}.$$

Classically this is the interference term for an $E1$ oscillator vibrating in the $\hat{x}'=\hat{z}$ direction shown in Fig. 3(b). The $\hat{x}'$ $E1$ oscillator feeds the channels "out of phase" (i.e., $+\hat{\epsilon}_x^{(0)}$ and $-\hat{\epsilon}_x^{(1)}$) and this leads to constructive interference. The factor $\sin(\theta/2)$ gives the geometrical projection of the oscillator perpendicular to the $\vec{k}$ channel. The fields from the third independent oscillator in the $\hat{y}'$ direction interfere destructively. Thus for an $E1$ Mössbauer or x-ray emitter located at a lattice site, there will be emission in a Laue channel of $\hat{\epsilon}_x$ radiation to a depth l_x ($\delta=0$), but the deeply penetrating $\hat{\epsilon}_y$ component is suppressed and there is no anomalous deep crystal emission.

An $M1$ source, however, feeds the channels "out of phase" with ϵ_y radiation, as shown in Fig. 3(b), which leads to constructive interference for the $\hat{\epsilon}_y$ component:

$$K_y(\delta=0)=-iK'(0)\sin(\theta/2) \quad (M1,\ M=0), \tag{20}$$

where

$$K'(0)=\frac{3}{8\pi}C(J_0\,1\,J_n;\ m_n0)\langle x_f|e^{-i\vec{k}\cdot\vec{r}}|x_0\rangle \times(\lambda\Gamma_\gamma)^{1/2}[\omega-E_m-\epsilon_0+E_0+\epsilon_f+\tfrac{1}{2}i\Gamma]^{-1}.$$

For the $\hat{\epsilon}_x$ radiation the interference is destructive:

$$K_x(\delta=0)=0 \quad (M1,\ M=0,\ \pm1). \tag{21}$$

The $\sin(\theta/2)$ factor in (20) again gives the projection of the oscillator perpendicular to the $\vec{k}$ and $\vec{k}_1$ channels.

Thus for an $M1$ source, there will be anomalous emission from deep crystal lattice sites in the Laue channels, and the radiation will be $\hat{\epsilon}_y$ polarized, i.e., everywhere tangent to the Kossel cone.

For an unsplit $E2$ source, with $\hat{z}$ axis taken as for the $M1$ case above, $\hat{\epsilon}_y$ radiation is fed constructively by the $M=\pm2$ transitions,

$$K_y(\delta=0)=K_y'(\pm2)\sin(\theta/2), \tag{22}$$

where

$$K'(\pm2)=\mp i\frac{5}{16\pi}C(J_0 2 J_n;\ m_n\pm2) \times\frac{\langle x_f|e^{i\vec{k}\cdot\vec{r}}|x_0\rangle(\lambda\Gamma_\gamma)^{1/2}}{\omega-E_n-\epsilon_0+E_0+\epsilon_f+\frac{1}{2}i\Gamma}.$$

Thus an $E2$ source also gives rise to anomalous emission from deep crystal lattice sites, and more generally this is true of any source of multipolarity $M1$ or higher.

B. Enhanced γ-ray sources

In two previous papers,[2,7] we have discussed some potentially important applications of Mössbauer-γ-ray diffraction studies. The feasibility of some of these experiments, e.g., the determination of the structure of biological molecules,[8,9] is controlled by the accessibility of intense well-collimated Mössbauer-γ-ray sources. These experiments have been impeded by the brightness limitations on the present sources of Mössbauer radiation. Hence a question of particular importance is whether coherence effects can lead to enhanced γ-ray emission in well-defined directions.

The principal factor limiting the intensity of the source is the self-absorption occurring within the source, which limits the effective source thickness to the order of the absorption length for the γ rays in the source material. However, as we have just seen, anomalous emission occurs for sources of multipolarity $M1$ or higher in the early development of a radioactive crystalline source. In this case the effective penetration depth for emission into the Laue channels is orders-of-magnitude greater

than the off-Bragg penetration depth, and it is possible to achieve an enhanced intensity in the Laue channels.

For a thick-crystal source containing a uniform distribution of parent isotopes, in the cases of "unsplit" $M1$ or $E2$ transitions the maximum intensity in the Kossel cone will be enhanced over the neighboring off-Bragg intensity by a factor of

$$E = \tfrac{1}{2}\sin^2(\theta/2)(1 - f_D(\theta))^{-1} + 1 \approx \tfrac{1}{4}\lambda\!\!\!^{-2}/\langle x^2\rangle + 1, \quad (23)$$

and will have a narrow collimation on the order of $\delta \lesssim 2\,\mathrm{Re}F^{00}_{yy}$, or

$$\delta\phi \lesssim 8\pi\lambda\!\!\!^{-2} n Z r_0/\sin\theta . \quad (24)$$

In (23) the first term is the ratio $|K_y|^2/|\hat{\epsilon}_y\cdot\vec{J}|^2$ of the intensity of the good $\hat{\epsilon}_y$ component emitted into a Kossel channel relative to the *total* intensity emitted into a neighboring off-Bragg point, times the enhancement of the penetration depth l_y/l_{0B}. This term gives the relative contribution to the intensity due to deep crystal emission. The second term, 1, represents the contribution of the first $(1/\alpha_y)$ layers from which all the radiation emerges. The enhancement of the Kossel line is determined by the ratio of the squared wavelength to the mean square vibrational displacement. As we have noted, the enhanced beam will be primarily polarized tangent to the Kossel cone, i.e., $\hat{\epsilon}_y$ polarized, the ratio of the intensity of the $\hat{\epsilon}_y$ component to the total intensity being

$$P_y = 1 - (2E)^{-1}, \quad (25)$$

where E is given by (23).

Finally, we note that these estimates hold for the recoil fraction as well as for the recoilless fraction.

In Table I, we list several Mössbauer isotopes and give the enhancement E, the polarization P, and the collimation $\delta\phi(\times\sin\theta)$ which can be achieved in the Laue channels at $T=0$. For Co^{57} in Fe at 4.3 K for $\theta = 20°$, these estimates give an enhancement of 4.4 which is 89% $\hat{\epsilon}_y$ polarized and collimated to $\delta\theta \lesssim 0.8\times10^{-4}$ rad ≈ 17 sec of arc about the Kossel cone. The exact theoretical curve for the intensity is shown in Fig. 5.

The maximum source enhancement shown in Table I is for the low-energy 8.4-keV γ ray of $_{69}Tm^{169}$ for which the source enhancement is 13.9 with 96% $\hat{\epsilon}_y$ polarization with beam collimation $\delta\theta \lesssim 48$ sec for $\theta = 20°$.

For $_{32}Ge^{73}$ the source enhancement is 5.0 with 90% $\hat{\epsilon}_y$ polarization and a collimation of $\delta\theta \lesssim 10$ sec for $\theta = 20°$. An interesting aspect of this case is that the anomalous-emission effect can be used to separate the 13.5-keV Mössbauer γ ray from the much more intense 10-keV x rays which follow internal conversion [the (x ray)/(γ ray) intensities $\approx 10^3$]. This can be accomplished by building a thick crystal source such that there are no active sources to a depth of 2×10^{-2} cm, which is 4 times the off-Bragg penetration depth of the x rays, $l_{0B} = 5\times10^{-3}$ cm. For the emitters located below this depth, the Mössbauer γ rays will be emitted from the crystal in the Laue channels by the anomalous-emission effect since the γ transition is $E2$. On the other hand, for the x rays there is no emission in Laue channels since the x-ray transition is $E1$. Furthermore the off-Bragg x-ray emission is down

TABLE I. Estimates for various Mössbauer isotopes for the enhancement E, the polarization P, the collimation $\delta\phi x\sin\theta$, and the lifetime $t_{1/2}$ for the "super" Kossel lines from thick uniformly doped crystal sources. We have taken $T=0$ in computing $\langle x^2\rangle$, and the resonance absorption cross sections σ_0' include the effect of the finite width of the source γ ray. The lifetime is computed for a 100%-enriched source.

Isotope	E_γ(keV)	$E=\frac{1}{4}\lambda\!\!\!^{-2}/\langle x^2\rangle+1$	$P=1-(2E)^{-1}$	$\delta\phi\times\sin\theta$ (sec)	$\sigma_0'(10^{-19}$ cm$^2)$	$\sigma_e(10^{-19}$ cm$^2)$	$\tau_{1/2}$	$t_{1/2}=\frac{\langle x^2\rangle}{\lambda\!\!\!^{-2}}\frac{\sigma_e}{\sigma_0'}\tau_{1/2}$
$_{26}Fe^{57}$	14.4	4.4	0.89	5.8	11.8	0.06	270 days (Co^{57})	0.10 days
$_{32}Ge^{73}$	13.5	5.0	0.90	3.4	0.011	0.15	76 days (As^{73})	62 days
$_{36}Kr^{83}$	9.3	2.7	0.82	5.0	9.4	0.10	83 days (Rb^{83})	0.13 days
$_{50}Sn^{119}$	23.9	3.7	0.87	1.4	6.6	0.03	38 h (Sb^{119})	0
$_{62}Sm^{149}$	22	2.3	0.78	1.8	2.0	0.08	106 days (Eu^{149})	0.82 days
$_{63}Eu^{151}$	21.6	2.4	0.79	1.6	1.2	0.09	120 days (Gd^{151})	1.6 days
$_{66}Dy^{161}$	25.7	2.0	0.75	1.8	5.3	0.07	6.9 days (Tb^{161})	0.02 days
$_{69}Tm^{169}$	8.4	13.9	0.96	16.5	1.0	0.35	32 days (Yb^{169})	0.22 days
$_{80}Hg^{201}$	32.1	1.5	0.67	1.9	0.05	0.08	74 h (Tl^{201})	59 h

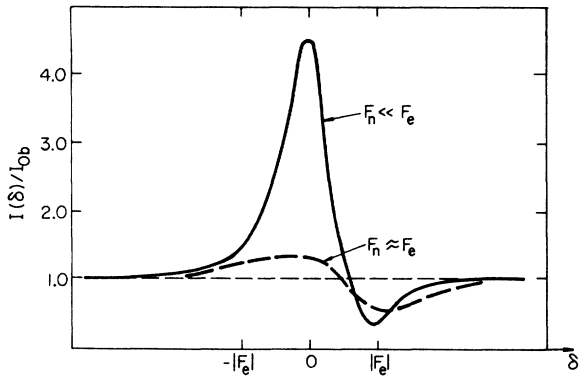

FIG. 5. Intensity of the Laue–Kossel line relative to the off-Bragg intensity for a thick Co^{57} source at 4.3°, $\theta = 20°$. δ gives the deviation from the exact Bragg condition. The solid line gives the intensity during the early development, and the dotted line gives the intensity when the nuclear and electronic scattering processes are of comparable magnitude. F_n and F_e give, respectively, the nuclear and electronic contributions to the planar scattering amplitude.

by a factor of 10^3 due to extinction. The γ-ray intensity in a Laue channel will then be about 4 times as intense as the off-Bragg x-ray intensity.[10]

C. Developed sources

The anomalous-emission effect is suppressed for the recoilless fraction in developed sources which contain an appreciable fraction of resonant nuclei. This suppression is due to increased resonant absorption which limits the Laue penetration depth, and to destructive interference which builds up as the scattering becomes more $M1$ (or $E2$, etc.) in character.

For a thick crystal containing a uniform distribution of Mössbauer atoms, in the case of an "unsplit" $M1$ Mössbauer transition, the Laue penetration depths for the recoilless fraction compared to the penetration depths at time $t = 0$ are

$$\left.\frac{l_y(\omega, t)}{l_y(\omega, 0)}\right|_{\delta=0} = \left[1 + \left(\frac{P(t)\sigma_n}{\sigma_e}\right)\left(\frac{1-\cos\theta}{1-f_D(\theta)}\right)\right]^{-1}, \tag{26}$$

$$\left.\frac{l_x(\omega, t)}{l_x(\omega, 0)}\right|_{\delta=0} = 1,$$

where $P(t)$ gives the fraction of resonant Mössbauer atoms and σ_n is the resonant absorption cross section given by Eq. (A4). From (26) we see that the penetration depth of the resonant $\hat{\epsilon}_y$ component is strongly suppressed due to the presence of the resonant $M1$ scatterers when $P\sigma_n > \sigma_e$, while the $\hat{\epsilon}_x$ component has the same Laue penetration depth as in the early development. This is an obvious result since the $\hat{\epsilon}_x$ polarization is the "good" polarization for the $M1$ scatterers, corresponding to an $\hat{\epsilon}_y$ polarization for $\vec{B}$, which can set up an $M1$ Borrmann effect (i.e., a cancellation of the B field at the lattice sites, so that there is no coupling to an $M1$ oscillator; hence there is a suppression of absorption). On the other hand, the $\hat{\epsilon}_y$ component will always have a nonvanishing B field at the nucleus, and hence there will be strong absorption.

Although $\hat{\epsilon}_x$ radiation has a much deeper Laue penetration depth than $\hat{\epsilon}_y$ radiation in a highly resonant $M1$ medium, there is no crystal emission of $\hat{\epsilon}_x$ radiation from a deep crystal lattice site (depth $\approx l_x$) because the Laue interference term K_x for $\hat{\epsilon}_x$ emission is destructive, as given by (21). (For *isotropic* $M1$ scattering, $F^{01}_{\lambda\lambda}/\beta_\lambda(\delta = 0) = +1$ so that the previous results (20) and (21) are still valid.) Thus there is no deep crystal emission from an $M1$ source in a predominantly $M1$ lattice, just as there is no deep crystal emission from an $E1$ source in an $E1$ lattice.

The emission of $\hat{\epsilon}_y$ radiation is constructive, as given by (20), and occurs to the Laue depth l_y given by (26). The penetration depth for the recoilless fraction will be down by $\frac{1}{2}$ when $P(t) \approx \lambda\!\!\!^{-2}\sigma_e/(\langle x^2\rangle\sigma_n)$, or after a time

$$t_{1/2} \approx \frac{\langle x^2\rangle}{\lambda\!\!\!^{-2}}\left(\frac{\sigma_e}{P_0\sigma_n}\right)\tau_{1/2}, \tag{27}$$

where $\tau_{1/2}$ is the half-life of the parent isotope.

For the $E2$ case the results are very similar. In particular, the expression for the ratio $l_y(\omega, t)/l_y(\omega, 0)$ is the same as that given in (26) for the $M1$ case, and hence the half-life $t_{1/2}$ of the anomalous-emission effect is again given by Eq. (27).

In Table I we give $t_{1/2}$ for the various isotopes listed with P_0 taken as 1 (i.e., a 100%-enriched source). For a source consisting initially of 10-at.% Co^{57} uniformly distributed in Fe at 4.3 K, then $t_{1/2} \approx 1$ day. Of course even for a highly developed source, the penetration depth l_y of $\hat{\epsilon}_y$ radiation at a Laue angle is greater than the off-Bragg penetration depth, $l_y/l_{0B} \approx (1-\cos\theta)^{-1}$, so that Laue emission can occur deeper within the crystal. For a uniformly populated thick crystal, there will be a weak enhancement, $E = \frac{5}{4}$, of the Laue intensity at exact Bragg over the off-Bragg background as shown in Fig. 5.

For the 8.4-keV γ ray of $_{69}Tm^{169}$ a 10-at.% source of Yb^{169} will have an anomalous-emission half-life of 5 days, while for the 13.5-keV γ ray of $_{32}Ge^{73}$, the half-life will be on the order of 70 days regardless of the concentration of As^{73}. This is because of the dominance of the electronic scattering absorption ($\sigma_e = 1.5\times10^{-18}$ cm^2) over the resonant scattering absorption ($\sigma_0' = 1.1\times10^{-19}$) which is suppressed by the very large internal conversion amplitude. For most cases, however, we see that the anomalous-emission effect rapidly decreases as the source develops.

D. Interstitial emission

The results are quite different if the emission occurs from an interstitial site rather than a regular lattice site. The distinction between lattice-site and interstitial emission has been discussed by Alexandrov and Kagan, [11] and has also been pointed out by Trammell. [12] A similar phenomenon occurs in the emission of x rays or electrons from crystals[13] and in the fluorescence scattering by foreign atoms. [14]

When the emission occurs from an interstitial, all the considerations of the Laue penetration depth are unchanged, but the interference effects are, naturally, quite different.

For lattice-site emission into a Laue channel, the relative phase factor $\exp[i(\vec{k}-\vec{k}_1)\cdot\vec{\rho}_j]$ between the two contributions to K_λ in (17) is $(+1)$. For an interstitial emitter, however, $\exp[i(\vec{k}-\vec{k}_1)\cdot\vec{\rho}_j]=(-1)^n$ for a Bragg condition $(\vec{k}-\vec{k}_1)\cdot\vec{d}_B = 2n\pi$, where $\vec{d}_B$ is the interplanar vector for a particular set of Bragg planes (for which $\vec{\rho}_j$ is an interstitial halfway between the planes). Thus for interstitial emission into *odd-order* Laue channels, the previous cases of destructive interference become constructive and vice versa.

For example, there will be very strong deep crystal emission for an $E1$ Mössbauer of x-ray emitter if the source is located at an interstitial position, and similarly there is deep emission from $M1$ sources in an enriched crystal if the sources are interstitial. However, the "interstitial effect" cannot be applied to obtain enhanced thick-crystal sources because the uniform distribution of "interstitials" then become "lattice sites."

Finally we note that the sensitivity of the emission pattern to the position of the emitter can be utilized in determining the location of the emitter within the unit cell. [11,12,14]

E. Magnetic Kossel effect

Quite aside from considerations relating to sources, the Kossel-line pattern itself is of considerable interest. The Kossel pattern exhibits the crystal symmetry and affords a sensitive measure of crystal parameters. In x-ray optics, Kossel pattern analysis has been used to make precision determinations of lattice parameters and orientation, and to determine the variation of the parameters with temperature and strain, the components of the strain tensor, and the degree of crystal perfection. [15] In Mössbauer-γ-ray optics these features are also present and a new phenomenon can occur: The Mössbauer scattering is sensitive to the direction of the magnetic field and electric-field-gradient tensor at the nucleus, and if the internal field "unit cell" is greater than the chemical unit cell, there will appear extra Kossel cones exhibiting the structure of internal field. We will call these additional lines "magnetic Kossel lines." Thus, for example, analysis of the magnetic Kossel-line pattern of rare-earth metals and alloys will permit accurate determinations of the spiral structures, and of their dependence on temperature and strain, which hitherto have been determinable only by neutron diffraction.

For example, if a magnetic crystal has a spiral axis $\hat{z}$ with a spiral angle θ, then there will be Bragg or Laue channels $\vec{k}$ and $\vec{k}_1$ open when $(\vec{k}-\vec{k}_1+n\vec{\theta})$ is equal to a reciprocal-lattice vector, where $\vec{\theta}=(\theta/d_s)\hat{z}$ and d_s is the interplanar distance along the spiral axis $\hat{z}$. The channels for $n\neq 0$ would normally be closed for x-ray scattering, so these channels uniquely exhibit the magnetic structure. These lines will, of course, only appear for "developed" crystals where there is appreciable resonant scattering, and only if the internal fields are strong enough to cause appreciable Zeeman splitting.

For the general "magnetic Kossel" case, one must resort to numerical methods for solving the dynamical equation. However, as a simple example, we consider a simple bcc antiferromagnetic crystal as shown in Fig. 6(a), and a symmetric magnetic Laue channel for which $(\vec{k}-\vec{k}_1)\cdot(\vec{R}_j^{\,\bullet}-\vec{R}_j^{\,+})=\pi$ where $\vec{R}_j^{\,\bullet}$ and $\vec{R}_j^{\,+}$ denote the positions of the two atoms in the jth *magnetic unit cell*. The chemical unit cell contains only one atom, and the wave vectors do not satisfy a Bragg condition for scattering from the chemical unit cells. We will assume that the γ transition is $M1$.

First we note that for an antiferromagnetic crystal magnetic Kossel cones will only occur for the

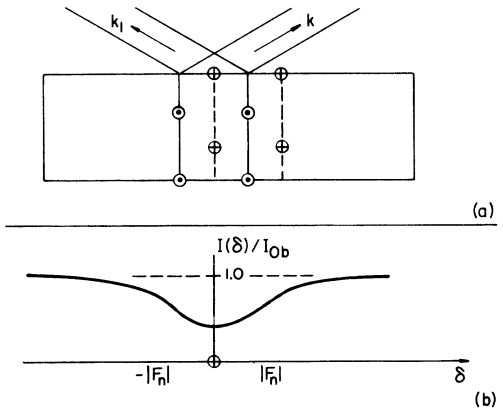

FIG. 6. (a) Schematic representation of the magnetic Kossel effect for a bcc antiferromagnetic crystal. The wave vectors satisfy $(\vec{k}-\vec{k}_1)\cdot(\vec{R}_j^{\,\bullet}-\vec{R}_j^{\,+})=\pi$, where $\vec{R}_j^{\,\bullet}$ and $\vec{R}_j^{\,+}$ denote the positions of the two atoms in the jth *magnetic unit cell*. (b) gives the intensity of the magnetic Kossel line relative to the off-Bragg intensity as a function of the deviation δ from the magnetic Bragg conditon.

$M=\pm1$ transitions. For an $M=0$ transition the scattering amplitude is invariant under the reversal of the quantization axis ($\hat{z}_H \to -\hat{z}_H$), therefore there is no distinction in the polarization or amplitude of the resonantly scattered waves from the two orientations ($\pm\hat{z}_H$). However, the scattering amplitude for an $M=\pm1$ transition is not invariant for $\hat{z}_H \to -\hat{z}_H$: The angular dependence of the scattering amplitude varies as

$$\hat{\epsilon}_y \cdot \vec{Y}^{(0)}_{1\pm1}(\vec{k}_f, +\hat{z}_H)\vec{Y}^{(0)}_{1\pm1}(\vec{k}_0, +\hat{z}_H)^* \cdot \hat{\epsilon}_y = [\hat{\epsilon}_y \cdot \vec{Y}^{(0)}_{1\pm1}(\vec{k}_f, -\hat{z}_H) \times \vec{Y}^{(0)}_{1\pm1}(\vec{k}_0, -\hat{z}_H)^* \cdot \hat{\epsilon}_y]^*$$

for the $M=\pm1$ transitions.

For a general point on the Kossel cone, the general solution accounting for the polarization mixing must be used, but for the point where $\vec{k}$ (and $\vec{k}_1$) are perpendicular to the magnetization axis $\pm\hat{z}_H$, the solution (4) or (4′) is valid. In this case the scattering amplitudes for the magnetic unit cell (taking R_j as origin) are given by

$$\begin{aligned} F^{00}_{yy} &= F^{11}_{yy} = 2F_e + 2F_{n(+1)} + 2F_{n(-1)}, \\ F^{00}_{xx} &= F^{11}_{xx} = 2F_e + 2F_{n(0)}, \\ F^{10}_{yy} &= -F^{01}_{yy} = 2i\sin\theta(F_{n(+1)} - F_{n(-1)}), \\ F^{10}_{xx} &= F^{01}_{xx} = 0, \end{aligned} \tag{28}$$

where F_e is given by $n\lambda d/\sin\phi_0$ times the electronic contribution (A4) to the forward-scattering amplitude and

$$F_{n(m)} = \frac{3\pi\lambda^2 ndP(t)\exp(-k^2\langle x^2\rangle)}{2^{|m|}(2J_0+1)\sin\phi_0} \times\left(\frac{\Gamma_\gamma}{\Gamma}\right)\sum_{m_0}\frac{C^2(J_0\,1\,J_n;\, m_0 M)}{x(m_0 M)-i} \tag{28′}$$

gives the planar coherent (forward-) scattering amplitude for the $\Delta J_z = M$ transitions for $M=0,\pm1$.

For our special orientation, the $\hat{\epsilon}_y$ polarization couples only to the $M=\pm1$ transitions, the $\hat{\epsilon}_x$ to $M=0$. According to (28), F^{10}_{xx} vanishes, and so there will be no magnetic scattering for the $M=0$ radiation, as we discussed above. For the $M=\pm1$ transitions, the unit-cell scattering amplitude F^{10}_{yy} for the magnetic Bragg case has a $\sin\theta$ dependence, so that the maximum effects will occur for large Bragg angles near $\pi/4$ (scattering angles θ near $\pi/2$). The maximum penetration depth for either an $M=+1$ or -1 resonance is

$$l_y(\delta=0) = d\{2\,\mathrm{Im}[F_e + (1-\sin\theta)F_{n(\pm1)}]\}^{-1} \quad \text{for } \omega \approx \Delta E(\pm1), \tag{29}$$

so that for a "magnetic Bragg angle" near $\pi/4$, the $M=\pm1$ resonances have a maximum penetration depth at Laue limited primarily by the photoelectric effect.

The emitted intensity is the incoherent sum of the squared amplitudes for emission from the $R^\bullet$ sites and the R^+ sites. In Fig. 6(b) we give a plot of the recoilless intensity for the $\pm\frac{1}{2}\to\pm\frac{3}{2}$, $M=\pm1$ transitions of Fe^{57} for Co^{57} in a thick antiferromagnetic crystal for $P(t)=0.1$, $\theta\simeq90°$. The curve shows the intensity of the $M=\pm1$ components versus δ, the deviation from the magnetic von Laue, for the case in which the shifts and resonances are identical at the $R^\bullet$ and R^+ sites (so that an $M=+1$ transition at an $R^\bullet$ site is exactly in resonance with an $M=+1$ transition at an R^+ site). For this case the magnetic Kossel line at the Laue angle occurs is a minimum in the recoilless intensity because of the destructive interference of the two waves feeding the Laue channels.

F. Sources with large Zeeman splitting

Magnetic information can also be obtained from the anomalous-emission effect: If there is large Zeeman splitting in the source then the frequency spectrum of the recoilless part of the Kossel line is very sensitive to the orientation of the internal magnetic field at the emitter with respect to the crystal planes and to the scattering plane containing $\vec{k}$ and $\vec{k}_1$. This occurs because a particular oscillator, i.e., a particular ΔJ_z transition, can only constructively feed $\hat{\epsilon}_y$ radiation into two channels for a limited range of orientations. As an example, if the magnetic field $\vec{H}$ lies in a crystal plane as shown in Fig. 3(b), then for the segment of the Kossel cone for which $\vec{H}$, $\vec{k}$, and $\vec{k}_1$ are coplanar, only the $M=0$ transition constructively feeds $\hat{\epsilon}_y$ radiation, and the recoilless fraction of the anomalous emission line will contain only the $M=0$ frequencies. On the other hand, for the segment of the cone for which the scattering plane is perpendicular to $\vec{H}$, only the $M=\pm1$ transitions contribute. These features are shown in Fig. 7 where we give the frequency spectrum of the recoilless fraction for $H\parallel\hat{z}$, $H\parallel\hat{z}+\hat{x}$, and $H\parallel\hat{x}$, where z bisects $\vec{k}$ and $\vec{k}_1$, and $\hat{y}=\hat{\epsilon}_y$, as shown in Fig. 3(b). The dotted lines give the relative intensities of the lines that would be obtained for the same orientation of $\vec{k}$ relative to $\vec{H}$ for off-Bragg emission.

Similar considerations also hold for developed sources although in this case the effect on the frequency spectrum of the relative orientation of the magnetic fields and crystal planes is much less pronounced.

G. Recoil fraction

The emitted radiation pattern for the recoil fraction is the same as that of the recoilless fraction coming from an *unsplit* source when the crystal is in its "*early development*," i.e., when there is essentially no resonant scattering within the lattice.

Thus for an $M1$ or higher-order-multipole emit-

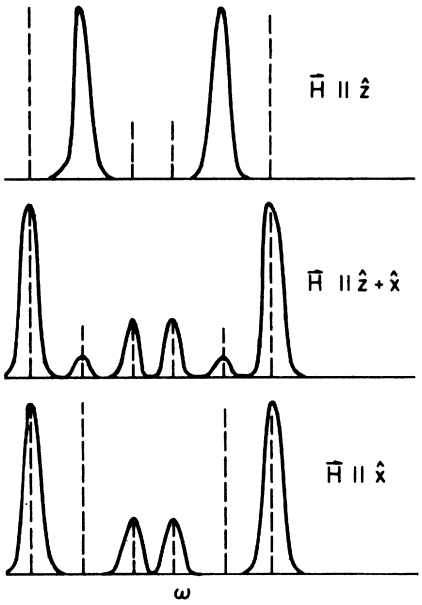

FIG. 7. The dark curves indicate the frequency spectrum in an anomalous emission Kossel line from a Zeeman split Fe^{57} source for three different orientations of the magnetic field. $\hat{x}$ lies perpendicular to the Bragg planes and $\hat{z}$ is parallel to the intersection of the Bragg planes and the scattering plane. We have assumed a symmetric Laue channel with $\theta = 20°$. The dashed lines indicate the frequency spectrum which would be observed at a neighboring off-Bragg point.

ter, the recoil fraction will exhibit the anomalous-emission effect, and the deep crystal emission for the *recoil* fraction will not disappear as the source develops, since the recoil radiation is not resonantly scattered.

For a thick-crystal source the recoil Kossel lines will be enhanced relative to the background and will be predominantly linearly polarized parallel to the cone. The enhancement E and polarization P_y are given by the previous expressions, Eqs. (23) and (25), and in particular the tabulated values in Table I hold for the recoil fraction. As the source develops, the recoil contribution will dominate.

Although the recoil fraction is, of course, unsuitable for Mössbauer studies, viewed as an x-ray source the recoil fraction is an extremely monochromatic (frequency spread $\sim \kappa\theta \lesssim 0.1$ eV) source of radiation which can be used for chemical structure studies in scattering experiments.

The recoil Kossel lines themselves can be analyzed to give precision determinations of lattice parameters of the crystal, and the change of these parameters under temperature and strain variations.

In magnetic crystals, the recoil fraction exhibits, of course, only the chemical cell Kossel lines. The recoil Kossel lines can thus serve as useful "bench marks" for the magnetic Kossel lines formed by the recoilless fraction; just as in neutron diffraction the scattering from the nuclei serves as a "bench mark" for the electronic magnetic scattering of the neutrons.

III. BRAGG CHANNELS

For the Bragg channels $\vec{k}$ is near a Bragg angle for some set of crystal planes and the wave field is determined by the $\vec{k}$ channel and a reflection channel $\vec{k}_1$, with $\vec{k}_1 = -g_1\hat{z} + \vec{k}_{xy} + \vec{\tau}_{xy}$, Eq. (1), which travels in the $-\hat{z}$ direction (i.e., $\vec{k}_1 \cdot \hat{z} < 0$) as shown in Fig. 8. The Bragg condition is now [Eq. (2) with $k_{1z} = -g_1$]

$$(g_0 + g_1)d = 2n\pi + 2\delta . \tag{30}$$

δ is again given by $\delta = (kd\sin\theta)\Delta\phi/(2\sin\phi_1)$ where θ is the scattering angle and $\Delta\phi$ is the deviation of the rocking angle ϕ_0 from the exact Bragg angle ϕ_0^B. $\vec{A}_M(\vec{k})$ is now given by Eq. (82) of IIIA in terms of the $\tilde{\mathcal{T}}$ and $\tilde{\mathcal{R}}$ matrices.

For simplicity, we shall again concentrate primarily on the case of no polarization mixing. The wave emitted from the crystal due to a decay at $\vec{R}_j$ is [Eq. (82) of IIIA]

$$\begin{aligned}\vec{A}'_M(\vec{k}) = {} & \tilde{D}^M_{m_j}(\vec{k}, \vec{k})e^{-i\vec{k}\cdot\vec{\rho}_j}\vec{J}_\perp(-\vec{k}, \omega; j) \\ & + \tilde{D}^M_{m_j}(\vec{k}, \vec{k}_1)e^{-i\vec{k}_1\cdot\vec{\rho}_j}\vec{J}_\perp(-\vec{k}_1, \omega; j) .\end{aligned} \tag{31}$$

As is the previous section, in the limit of no polarization mixing the $\tilde{D}$ matrices of (31) are diagonal, as are the $\tilde{\mathcal{T}}$ and $\tilde{\mathcal{R}}$ matrices of Eq. (82) of IIIA. Substituting Eqs. (43) and (47) of II for the $\tilde{\mathcal{T}}$ and $\tilde{\mathcal{R}}$ matrices into Eq. (82) of IIIA, we obtain after some algebra

$$(\tilde{D}^M_{m_j}(\vec{k}, \vec{k}))_{\lambda\lambda} = Q_\lambda^{-1}\exp[iM_j(\alpha_\lambda + \beta_\lambda + g_0 d - \delta)], \tag{32}$$

$$\begin{aligned}(\tilde{D}^M_{m_j}(\vec{k}, \vec{k}_1))_{\lambda\lambda} = {} & im_\lambda^j F^{01}_{\lambda\lambda} Q_\lambda^{-1} \\ & \times \exp[iM_j(\alpha_\lambda + \beta_\lambda + g_0 d - \delta)],\end{aligned} \tag{33}$$

where, as in Sec. II, $\lambda = x$ or y or $\lambda = \hat{\epsilon}_{LM\lambda}$ for the

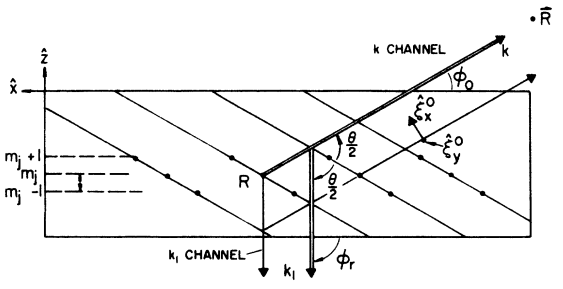

FIG. 8. Schematic representation of a Bragg Kossel channel.

various cases of no polarization mixing, and F' is given by (7) and (8), and

$$\alpha_\lambda = \tfrac{1}{2}(F^{00}_{\lambda\lambda} - F^{11}_{\lambda\lambda}),$$
$$\beta_\lambda = (\eta_\lambda^2 - F^{01}_{\lambda\lambda}F^{10}_{\lambda\lambda})^{1/2}, \quad \mathrm{Im}\beta_\lambda > 0, \tag{34}$$
$$\eta_\lambda = \delta + \tfrac{1}{2}(F^{00}_{\lambda\lambda} + F^{11}_{\lambda\lambda}),$$

and where

$$Q_\lambda = \left(\frac{\eta_\lambda + \beta_\lambda}{2\beta_\lambda}\right)\left[1 - e^{2iM_j\beta_\lambda}\left(\frac{\eta_\lambda - \beta_\lambda}{\eta_\lambda + \beta_\lambda}\right) + im_\lambda^j(\eta_\lambda - \beta_\lambda)(1 - e^{2iM_j\beta_\lambda})\right], \tag{35}$$

$$m_\lambda^j = \frac{i(1 - e^{2im_j\beta_\lambda})}{(\eta_\lambda + \beta_\lambda) - e^{2im_j\beta_\lambda}(\eta_\lambda - \beta_\lambda)}.$$

As before, $M_j = M - m_j$ gives the number of layers below the top surface of the emitter, and m_j gives the number of layers above the bottom surface. For an emission near a Bragg angle from a site $\vec{R}_j$ close to the bottom surface (such that $m_j\beta_\lambda \ll 1$), then $m_\lambda^j \doteq m_j$; while for a thick crystal (for which we will generally have $m_j\beta_\lambda \gg 1$), then $m_\lambda^j \doteq i(\eta_\lambda + \beta_\lambda)^{-1}$. The denominator Q_λ also has a simple dependence for thick or thin films: $Q_\lambda = 1$ for thick crystals ($m_j\beta_\lambda \gg 1$, but no restriction on M_j), and $Q_\lambda = 1 - iM_j(\eta_\lambda - \beta_\lambda)$ for thin films ($M_j\beta$, $m_j\beta \ll 1$).

Just as in the Laue case, we see from Eq. (31) that the wave emitted in the Bragg channel is the superposition of two waves: $\tilde{D}(\vec{k}, \vec{k})$ again gives the amplitude of the wave in the $\vec{k}$ channel at the crystal surface which arises from the direct feeding of the $\vec{k}$ channel at $\vec{R}_j$, while $\tilde{D}(\vec{k}, \vec{k}_1)$ gives the wave in the $\vec{k}$ channel at the crystal surface which arises, due to Bragg scattering within the medium, from the feeding of the $\vec{k}_1$ channel at $\vec{R}_j$. Again the amplitudes and phases with which the two channels are being fed at R_j are given by $\vec{J}^{f0}(-\vec{k}_\tau, \omega; j)e^{-i\vec{k}_\tau\cdot\vec{\rho}_j}$ for $\vec{k}_\tau = \vec{k}, \vec{k}_1$.

In the remainder of this section we will restrict our attention to the thick-crystal limit [$Q_\lambda = 1$, $m_\lambda^j = i/(\eta_\lambda + \beta_\lambda)$], which will hold in almost all cases. In this limit the expression for the emitted wave simplifies to

$$\vec{A}'_M(\vec{k}) = \sum_{\lambda = x,y} \hat{\epsilon}_\lambda^{(0)} K_\lambda(\delta, \omega; R_j) \times \exp[iM_j(\alpha_\lambda + \beta_\lambda + gd - \delta)], \tag{36}$$

where

$$K_\lambda = \hat{\epsilon}_\lambda^{(0)} \cdot \vec{J}^{f0}(-\vec{k}, \omega; j)e^{-i\vec{k}\cdot\vec{\rho}_j} - \left(\frac{F^{01}_{\lambda\lambda}}{\eta_\lambda + \beta_\lambda}\right)\hat{\epsilon}_\lambda^{(1)} \cdot \vec{J}^{f0}(-\vec{k}_1, \omega; j)e^{-i\vec{k}_1\cdot\vec{\rho}_j}. \tag{37}$$

As before, the factor K_λ in (36) gives the effect of the interference of the two waves in the $\vec{k}$ channel which occur because the source feeds both the $\vec{k}$ and $\vec{k}_1$ channels, and the maximum penetration depth l_λ for the ϵ_λ polarization is determined by the $\exp[iM_j(\alpha_\lambda + \beta_\lambda)]$ factor, i.e.,

$$l_\lambda(\delta) = d[\mathrm{Im}(\alpha_\lambda + \beta_\lambda)]^{-1}. \tag{38}$$

The nature of the interference and penetration depth of Bragg emission Kossel lines is quite different from the Laue case. As shown in Figs. 9(a) and 9(c) for a symmetric Bragg channel, the interference terms $K_\lambda(\delta)$ goes through a sharp maximum or minimum on the "lower" edge ($\delta = RF^{01}_{\lambda\lambda} - RF^{00}_{\lambda\lambda}$) of the "total" reflection region ($\delta + RF^{00}_{\lambda\lambda}) \propto \pm RF^{01}_{\lambda\lambda}$, with a width on the order of $RF^{01}_{\lambda\lambda}$. The destructive interference occurs if the two channels are fed "in phase" (i.e., both with $+\hat{\epsilon}_y$; or $+\hat{\epsilon}_x^{(1)}$ and $+\hat{\epsilon}_x^{(0)}$) while the maximum occurs if the channels are fed "out of phase." As noted before in connection with Fig. 3, for an $E1$ or $M1$ source only the linear component of the oscillator bisecting $\vec{k}$ and $\vec{k}_1$ will lead to constructive interference for a lattice-site emitter, and the amplitude

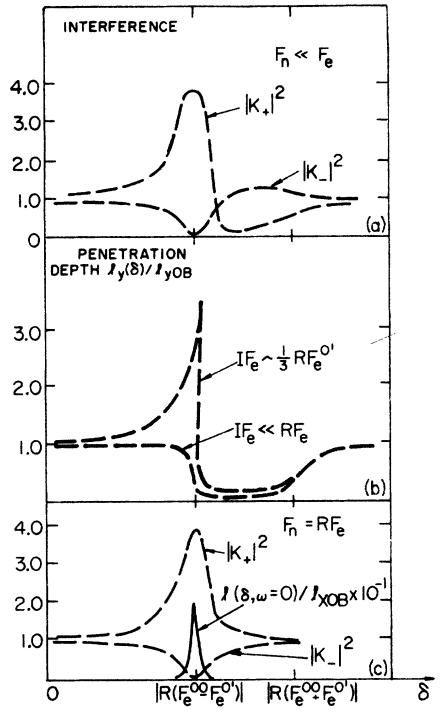

FIG. 9. (a) The interference term $|K|^2$ as a function of the deviation δ from exact Bragg condition for a Bragg reflection channel in the limit that the nuclear scattering is small compared to the electronic. The K_+ (K_-) curve is for constructive (destructive) interference between the direct and reflected waves. (b) The penetration depth as a function of δ for two different ratios between the imaginary part of the forward scattering amplitude and the real part of the $\vec{k}_1 \to \vec{k}$ scattering amplitude. (c) Plots of the interference $|K|^2$ and the penetration depth $l_x(\delta)$ for the recoilless radiation when the nuclear and electronic scattering are of equal magnitude.

for the process is decreased by the geometrical factor $\sin(\theta/2)$. Thus the interference term for *lattice-site* emission is primarily a sharp minimum. For *interstitial* emission the nature of the interference is reversed and will be primarily constructive.

The behavior of the pepetration depth l_λ depends upon the strength of the absorption relative to the strength of the coherent elastic scattering. As shown in Fig. 9(b), for a weakly absorbing crystal (i.e., $IF_{\lambda\lambda}^{00} \ll RF_{\lambda\lambda}^{01}$) the penetration depth decreases from its off-Bragg depth and abruptly minimizes in the total reflection region. This sharp cutoff of the penetration depth in the early development of a crystal is well known in x-ray optics and is made obvious by the reciprocity principle, since the penetration depth of an external plane wave is reduced sharply in this region due to the strong elastic scattering from the electrons. On the other hand, if there is relatively strong absorption (i.e., $IF_{\lambda\lambda}^{00} \lesssim RF_{\lambda\lambda}^{01}$), then the penetration depth maximizes just at the lower edge of the total reflection region ($\delta = RF_{\lambda\lambda}^{01} - RF_{\lambda\lambda}^{00}$) and then abruptly minimizes. The enhancement of the maximum penetration depth relative to that off-Bragg case is

$$l_\lambda^*/l_{0B} = \left((1-a_\lambda)\left\{\left[\left(\frac{1+a_\lambda}{2}\right)^2 + b_\lambda^2\right]^{1/2} + \left(\frac{1+a_\lambda}{2}\right)\right\}\right)^{1/2}, \tag{39}$$

where $a_\lambda = IF_{\lambda\lambda}^{01}/(IF_{\lambda\lambda}^{00})$ and $b_\lambda = RF_{\lambda\lambda}^{01}/(IF_{\lambda\lambda}^{00})$. In the "early development" of a crystal when the scattering is primarily electronic and we generally have $a_\lambda \ll b_\lambda$, then

$$l_y^*/l_{0B} = \left(\frac{4\pi F(\theta) f_D(\theta) r_0 (1 - f_D(\theta))}{k\sigma_e}\right)^{-1/2}$$

$$\approx \left(\frac{\lambda\sigma_e}{8\pi r_0 \langle x^2\rangle_T F(\theta) f_D(\theta) \sin^2(\theta/2)}\right)^{1/2} \tag{40}$$

and

$$l_x^*/l_{0B} = \left(\frac{4\pi F(\theta) f_D(\theta) \cos\theta\, r_0 (1 - \cos\theta f_D(\theta))}{k\sigma_e}\right)^{-1/2}$$

$$\approx \left(\frac{\sigma_e}{8\pi\lambda r_0 F(\theta) f_D(\theta) \cos\theta \sin^2(\theta/2)}\right)^{1/2}, \tag{40'}$$

where the notation is that of Eq. (12).

For Co^{57} in Fe, $\theta = 20°$, $T = 4.3°$, there is a weak enhancement, $E = 1.7$, of the $\hat{\epsilon}_y$ penetration depth, while there is no enhancement for the $\hat{\epsilon}_x$ radiation.

On the other hand, for a strongly resonant sample $a_\lambda \gg b_\lambda$, and the maximum penetration depth is given by

$$l_\lambda^*/l_{0B} \cong (1 - a_\lambda^2)^{-1/2}. \tag{41}$$

In this case the penetration depth at the (effective) Bragg condition can be much greater than off Bragg, as shown in Fig. 9(c) (where for a Fe crystal enriched with $P = 10$-at.% Fe^{57} and for a scattering angle $\theta = 20°$, $l_x^*/l_{0B} = [4\sin^2(\theta/2)\sigma_e/P\sigma_n]^{-1/2} \simeq 13$). This occurs because when a crystal containing resonant nuclei is excited at a Bragg angle, there is an enhancement of the effective coherent elastic radiative width and a consequent suppression of absorptive and inelastic processes.[2,16–19]

If the absorption is normally very strong (i.e., $\Gamma \gg \Gamma_\gamma$), which is often the case for Mössbauer atoms, then the suppression of the absorption processes at Bragg angles causes enhanced transmission even though reflection is also strongly increased. It should be noted, however, that the increase of the penetration depth here is much less than the increase in the Laue case, so that there is no anomalous deep crystal penetration. For the iron example just considered, the enhancement in the Laue case is [from Eqs. (14) and (26)]

$$l_x^*/l_{0B} = \frac{1}{2\sin^2(\theta/2)} \frac{P\sigma_n}{\sigma_e} \simeq 3.4\times 10^2.$$

Returning to the early stage of the development of a source, we see that there is no anomalous-emission effect for Bragg Kossel emission, and there is no strong dependence on the multipolarity of the emitter. This is a consequence of the gen-

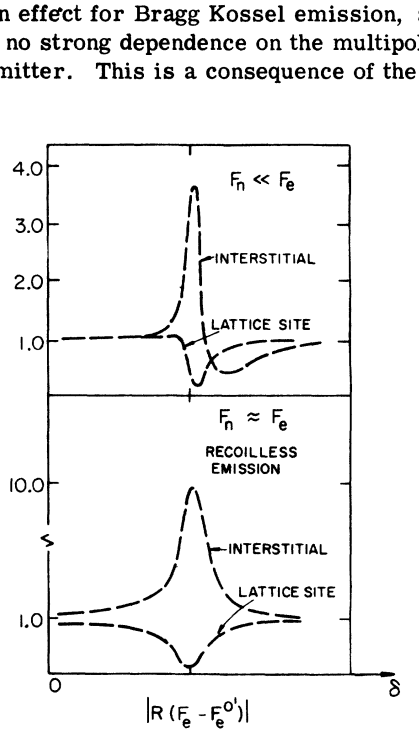

FIG. 10. Rocking curves for the Bragg–Kossel channel intensity relative to the off-Bragg intensity for a thick Fe crystal source uniformly populated with Fe^{57} emitters at lattice sites or interstitials. The interstitial curves are calculated assuming that the fraction of interstitial emitters is very small. The curves $F_n \ll F_e$ are for the "early development," and the curves $F_n \approx F_e$ are for the recoilless emission in a developed source.

erally destructive nature of the interference term, and, more importantly, because there is no anomalous deep crystal penetration. As shown in Fig. 10 for a uniformly doped thick-crystal source, the Bragg Kossel lines will be characterized primarily by a minimum if the source is at a lattice site and by a maximum if the source is interstitial. If the source exhibits strong Zeeman splitting, a particular resonance frequency can exhibit a maximum in the Kossel-line region though the source is at a lattice site. As in the Laue case, which resonance frequency will exhibit the maximum depends on the orientation of the magnetic field with respect to the crystal planes.

Magnetic Kossel lines will also occur for the Bragg case for resonant magnetic crystals which have a larger magnetic (or EFG) unit cell than chemical unit cell. The general considerations and features are the same as for the Laue case.

A. Phase determination

The problem of determining the structure of complex molecules by x-ray diffraction is greatly complicated by the fact that the reflected intensity only gives the magnitude of the unit-cell scattering factor and *not* the phase. For this reason, considerable effort has been devoted to devising methods for extracting phase information.

Typically one utilizes the interference between *scattered* waves to determine the phase of the unit-cell scattering amplitude relative to the phase of the wave scattered from a limited number of impurity sites. For example, in Mössbauer diffraction one substitutes resonant Mössbauer atoms into the sample to be studied. Because of the exceedingly sharp resonance, it is then possible to vary the phase and amplitude of the resonantly scattered wave by Doppler-shifting with negligible variation in the nonresonant electronically scattered wave. Consequently the interference between the waves is easily varied in a controlled manner. As discussed by Black,[8] and as demonstrated by Parak *et al.*,[9] it is then possible to extract the phase of the chemical structure factor of the unit cell relative to the structure factor due to the resonant scattering at the Mössbauer sites. The problem is then reduced to determining the relative positions of the Mössbauer atoms within the unit cell. In practice, of course, these experiments are very difficult and, as discussed by Parak *et al.*,[9] there are formidable problems in applying this procedure to the analysis of significant biological molecules.

Although Kossel-line studies have been used to make precision determinations of crystal symmetries and lattice parameters,[15] Kossel-line analysis apparently has not been utilized to obtain phase information. The purpose of this section is to point out that Kossel-line analysis offers an alternative method for phase determination: The interference of the direct wave emitted in a given direction with that Bragg reflected into this direction (Fig. 8) allows the phase of the latter to be obtained from the intensity distribution within the Kossel line, as in the holographic technique where phase information is obtained by "beating" the diffracted wave with a primary reference wave.

We recognize that this procedure for obtaining phase information will also present formidable experimental problems. In particular, accurate intensity measurements of the various Kossel lines are difficult because of the low contrast and narrow widths of the Kossel lines. Typically for a perfect crystal the Kossel lines will only be a few times background intensity at most, and with an angular width of a few second of arc.

To be explicit, we consider a thick molecular crystal with γ-ray sources (radioactive isotopes, or, e.g., resonant Mössbauer atoms whose incoherent scattering when illuminated constitute sources) substituted into the unit cells near the top surface of the crystal [within the total reflection extinction depth $l_y = d/\mathrm{Im}(\alpha_y + \beta_y)$]. From Eq. (42) of IIIA and Eq. (36), the emitted flux in a Bragg–Kossel line region is then given by

$$I(\delta) = \sum_{\lambda=x,y} N(t)\left(\frac{1}{2J_n+1}\right)\frac{1}{\nu}\sum_{\rho'}\sum_{f,0}\int d\omega\,\frac{\omega_0}{4\pi^2\hbar c} \times\left|1-\frac{F^{01}_{\lambda\lambda}}{\eta_\lambda+\beta_\lambda}S_\lambda(\rho')\right|^2 |\vec{\epsilon}^{(0)}_\lambda\cdot\vec{J}^{f0}(-\vec{k},\omega;\rho')|^2. \tag{42}$$

where

$$S_\lambda(\rho') = e^{-i(\vec{k}_1-\vec{k})\cdot\vec{\rho}'}\frac{\hat{\epsilon}^{(1)}_\lambda\cdot\vec{J}^{f0}(-\vec{k}_1,\omega;\rho')}{\hat{\epsilon}^{(0)}_\lambda\cdot\vec{J}^{f0}(-\vec{k},\omega;\rho')}. \tag{43}$$

In (42) $N(t)$ is the number of γ-ray decays per second in the crystal, we have assumed that there are ν emitting sites per unit cell located at positions $\vec{\rho}'$, and $2J_n+1$ is the multiplicity of the excited Mössbauer level. The factors α_λ, β_λ, and η_λ are given by (34). We assume that the scattering is primarily Rayleigh scattering from the atomic electrons, then the planar scattering amplitudes are given by

$$\begin{aligned} F^{01}_{\lambda\lambda} &= (KC_\lambda/\sin\varphi_1)A_h e^{i\Phi_h}, \\ F^{10}_{\lambda\lambda} &= (KC_\lambda/\sin\varphi_0)A_h e^{-i\Phi_h}, \\ F^{00}_{\lambda\lambda} &= (K/\sin\varphi_0)\sum_\rho f^{(\rho)}_{\lambda\lambda}(\vec{k},\vec{k}), \\ F^{11}_{\lambda\lambda} &= (K/\sin\varphi_1)\sum_\rho f^{(\rho)}_{\lambda\lambda}(\vec{k}_1,\vec{k}_1), = (\sin\varphi_0/\sin\varphi_1)F^{00}_{\lambda\lambda}, \end{aligned} \tag{44}$$

where $\lambda = x$ or y, $C_y = 1$, $C_x = \cos\theta$, $K = n\lambda_0 d$, n is the density of unit cells, θ is the scattering angle, and

$$A_h e^{i\Phi_h} = \sum_\rho f^{(\rho)}_{\lambda\lambda}(\vec{k},\vec{k}_1)e^{-i(\vec{k}-\vec{k}_1)\cdot\vec{\rho}} \tag{45}$$

is the unit-cell scattering amplitude, with A_h the modulus and ϕ_h the phase, for the Bragg reflection h.

We take the sources to be isotropic $M1$ emitters, and for simplicity we first assume only one emitter per unit cell located at $\rho' = 0$; then we find from Eqs. (A2′) and (42)–(44) that the intensity of the $\hat{\epsilon}_\lambda$ component in the Bragg–Kossel region relative to the off-Bragg intensity is

$$\frac{I_\lambda(\Delta\varphi)}{I_{\lambda 0B}} = 1 - C_\lambda^{-1}\cos\theta\left(\frac{\sin\varphi_0}{\sin\varphi_1}\right)^{1/2} \times\left(e^{i\phi_h}\left\{\frac{\Delta\varphi'}{w_{\lambda h}} + \left[\left(\frac{\Delta\varphi'}{w_{\lambda h}}\right)^2 - 1\right]^{1/2}\right\}^{-1} + \text{c.c.}\right) + \frac{\sin\varphi_0}{\sin\phi_1}\left|\frac{\Delta\varphi'}{w_{\lambda h}} + \left[\left(\frac{\Delta\varphi'}{w_{\lambda h}}\right)^2 - 1\right]^{1/2}\right|^{-2}. \quad (46)$$

In (46) ϕ_h is the phase of the structure factor for the Bragg reflection "h"; $w_{\lambda h}$ is half the angular width of the total reflection region, the thickness of the Kossel cone, for this reflection; $\Delta\varphi'$ is the difference of the cone angle of $\hat{k}$ and that of the center of the Kossel cone taken in the sense that $\Delta\varphi' > 0$ for directions lying within the cone (as is well known $\Delta\varphi'$ differs from $\Delta\varphi$, the deviation from the "kinematic" Bragg angle, by a few seconds of arc because of refraction); finally θ is the scattering angle $\measuredangle(\hat{k}_1, \hat{k})$.

Explicitly,

$$w_{\lambda h} = n\lambda_0^2 A_h C_\lambda (\pi\sin\theta)^{-1}(\sin\varphi_1/\sin\varphi_0)^{1/2}, \quad (47)$$

and $\Delta\varphi' = \Delta\varphi + n\lambda_0^2 A_0 (2\pi\sin\theta)^{-1}(\sin\varphi_0/\sin\varphi_1 + 1)$, where the second term represents the deviation of the center of the total reflection region from the kinematic Bragg angle, with A_0 the forward-scattering structure factor [$\hat{k} = \hat{k}_1$ in (45)]. A_0 has a small positive imaginary part.

In Eq. (46) the first term, 1, represents the intensity of the wave emitted directly into the $\hat{k}$ direction, the last term that Bragg reflected into this direction, and the second term the interference of these two waves.

For $|\Delta\varphi'| < w_{\lambda h}$ the reflected wave has modulus $(\sin\varphi_0/\sin\varphi_1)^{1/2}$ [hence total reflection, since waves emitted in the solid angle $d\Omega_1$ are Bragg reflected into solid angle $d\Omega_0 = (\sin\varphi_1/\sin\varphi_0)d\Omega_1$]; its phase is fixed by the stipulation that $\text{Im}[(\Delta\varphi'/w_{\lambda h})^2 - 1]^{1/2} > 0$. The phase of the reflected wave amplitude

$$r_\lambda(\Delta\varphi') \equiv -e^{i\phi_h}[\eta' + (\eta'^2 - 1)^{1/2}]^{-1}(\sin\varphi_0/\sin\varphi_1)^{1/2}, \quad (48)$$

with $\eta' \equiv \Delta\varphi'/w_{\lambda h}$ is thus ϕ_h for $\eta' < -1$ (outside the Kossel cone), $\phi_h + \pi$ for $\eta' > +1$ (inside the Kossel cone), and $\phi_h + \pi - \tan^{-1}[(1-\eta'^2)^{1/2}/\eta']$, for $|\eta'| < 1$ (within the width of the Kossel line). The phase of r_λ increases by π as η' goes from -1 to $+1$, and it is this that allows ϕ_h to be inferred from intensity measurements.

If $\cos\theta$ is small and $\varphi_0 = \varphi_1$ (Bragg planes parallel to the surface) then (46) becomes

$$I_\lambda(\Delta\varphi')/I_{\lambda 0B} = |1 - e^{i\phi_h}[\eta' + (\eta'^2 - 1)^{1/2}]^{-1}|^2. \quad (49)$$

If then $0 < \phi_h < \pi$, $I_\lambda(\Delta\varphi')/I_{\lambda 0B}$ will go to zero at some point in the total reflection region $|\eta'| < 1$, whereas if $\pi < \phi_h < 2\pi$ it will become 4 at some point in this region. In the general case, we have for $|\eta'| > 1$

$$\frac{I(\Delta\varphi')}{I_{0B}} = 1 - 2C_\lambda^{-1}\cos\theta\left(\frac{\sin\varphi_0}{\sin\varphi_1}\right)^{1/2} \times[\eta' + (\eta'^2 - 1)^{1/2}]^{-1}\cos\phi_h + \left(\frac{\sin\varphi_0}{\sin\varphi_1}\right)[\eta' + (\eta'^2 - 1)^{1/2}]^{-2}, \quad (50)$$

where the radical is positive if $\eta' > 1$ and negative if $\eta' < -1$; and for $|\eta'| < 1$

$$\frac{I(\Delta\varphi')}{I_{0B}} = 1 - 2C_\lambda^{-1}\cos\theta\left(\frac{\sin\varphi_0}{\sin\varphi_1}\right)^{1/2} \times[\eta'\cos\phi_h + (1-\eta'^2)^{1/2}\sin\phi_h] + \frac{\sin\varphi_0}{\sin\varphi_1}. \quad (50')$$

Comparing (50) and (50′) we see that the antisymmetric term (about $\eta' = 0$) $\propto \cos\theta\cos\phi_h$, whereas the symmetric interference term $\propto \sin\phi_h\cos\theta$.

In Fig. 11 we plot $I(\Delta\varphi')/I_{0B}$ (with $\cos\theta \doteq 1$, $\varphi_1 = \varphi_0$) as a function of η', for several values of ϕ_h. The shape of the line is clearly a very sensitive function of ϕ_h, and the line usually contains a bright ring (intensity maximum) and a dark ring relative to background. In a *centrosymmetric* crystal, with the emitting atom at a center of symmetry, $\phi_h = 0$ or π. Then if $\theta < \pi/2$ the Kossel cone will have an inner dark ring and an outer bright ring if $\phi_h = 0$ and the opposite if $\phi_h = \pi$. If $\theta > \pi/2$ there is a reversal of order. *Thus ϕ_h can be obtained for all the reflections of a centrosymmetric molecule by qualitative examination of the Kossel cones recorded on a photographic plate.*

It is apparent from (50), (50′), or Fig. 11 that high resolution measurements of the Kossel-cone structure would determine A_h and ϕ_h. Unfortunately the widths of these lines, w_h [Eq. (47)], are approximately a few seconds of arc. To obtain the Kossel lines with a resolution approximating the linewidth would require that the detector be located at a distance $\sim 10^5 \times$(linear dimension of the crystal). Practically, A_h should be determined by x-ray-diffraction techniques, then ϕ_h can be determined by measurements using "poor" resolution, say 10–50 sec of arc.

Consider the integrated relative brightness excess

$$S'_{2\Delta} = \sum_\lambda \int_{-\Delta}^{\Delta}[I_\lambda(\Delta\varphi') - I_{\lambda 0B}]d(\Delta\varphi') \Big/ \sum_\lambda \int_{-\Delta}^{\Delta} I_{\lambda 0B}\, d(\Delta\varphi')$$

$$= (4\Delta)^{-1} \sum_{\lambda} \int_{-\Delta}^{\Delta} \left(\frac{I_\lambda(\Delta\varphi')}{I_{\lambda 0B}} - 1 \right) d(\Delta\varphi')$$

$$\doteq \frac{w_{yh}}{2\Delta} \frac{\sin\varphi_0}{\sin\varphi_1} \times \left\{ \tfrac{4}{3}(1+\cos\theta) - \pi \cos\theta \left(\frac{\sin\varphi_1}{\sin\varphi_0} \right)^{1/2} \sin\phi_h \right\}, \quad \Delta \gg \omega_h \tag{51}$$

where w_{yh} is given by (47) with $\lambda = y$. If A_h is known, then measurement of the integrated intensity in an angular region 2Δ centered on the Kossel line will determine $\sin\phi_h$ through (51). The correct quadrant (first or second, third or fourth) can then be determined by qualitative observation of the dark–bright ring order (Fig. 11) as in the case of the centrosymmetric crystal. The value of the expression in $\{\ \}$'s in (51) is denoted by S in Fig. 11. We see that it is a sensitive function of ϕ_h varying from a minimum of $S = -0.47$ for $\phi_h = \pi/2$, to a maximum of $S = +5.81$ for $\phi_h = 3\pi/2$.

As an example $2w_h = 2.6$ sec of arc for the (020) Bragg reflection in $K_3Fe(CN)_6$.[9] If we take $2\Delta = 10$ sec then (51) gives $S'_{2\Delta} = 0.33$, an excess counting rate over that of background of 33 counts per hundred. In fact, ϕ_h is zero for this reflection, but if instead ϕ_h were, e.g., $\pi/2$ or $3\pi/2$, then one would measure excess relative intensities $S'_{2\Delta} = -0.08$ or $+0.74$, respectively. For the (800) reflection in myoglobin[21] $2w_h = 0.52$ sec of arc. Again taking $2\Delta = 10$ sec arc we get $S'_{2\Delta} = 0.07$. ϕ_h is also zero for this reflection. If it were $\pi/2$ or $3\pi/2$, then $S'_{2\Delta}$ would be -0.013 or $+0.14$, respectively.

Naturally this method of phase determination for large molecules will present difficult experimental problems. The intensities and contrast are low, and the lines are very narrow. On the other hand, if the emitted radiation is recorded, e.g., on a photographic plate, one would obtain simultaneously the Kossel cones from all (or a large fraction of) the Bragg reflections. This *does* represent a straightforward method for phase determination by what is essentially a holographic technique, and it may be the best way to obtain the phases for large molecules.

In the above development we have assumed a single emitting site in each unit cell fixed at $\vec{\rho}\,' = 0$. It is simple to take the zero point and thermal motion of the emitters into account and to allow as well for several emitting sites in the unit cells.

We first note that the Kossel cones of the Doppler-shifted (recoil) γ rays will generally differ in angular position from those of the recoilless γ rays by less than the width of the Kossel cone, w_h. This comes from the fact that when a phonon is created or absorbed in the radiation process it will generally shift the energy of the γ ray by less than about 0.1 eV. If the individual atoms are to be resolved than γ-ray wavelengths less than 1 Å or γ-ray energies greater than 10^4 eV are required. Thus $\delta k/k \lesssim 10^{-5}$, and since the shifts in positions of the Bragg angles $\delta\varphi_B \approx \delta k/k$ we obtain $\delta\varphi_B \lesssim 10^{-5}$ rad ≈ 1 sec arc $\lesssim \omega_h$.

If now there are ν emitting sites in each unit cell, the formulas we have obtained for the relative intensities must be modified according to the following substitutions

$$\cos\phi_h \to \mu\cos(\phi_h + \phi_n), \qquad \sin\phi_h \to \mu\sin(\phi_h + \phi_n), \tag{52}$$

where $\mu e^{i\phi_n}$ is the structure factor for the emitting sites,

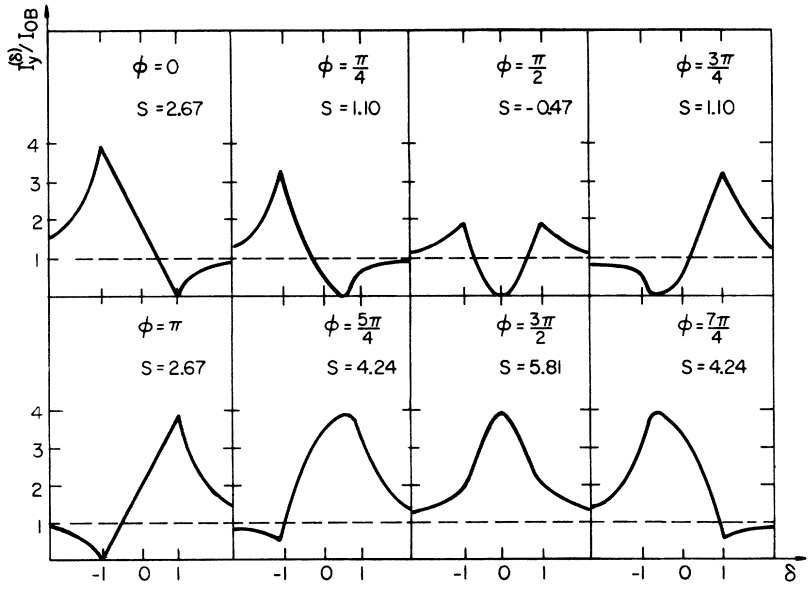

FIG. 11. Rocking curves for the Kossel-line intensity (relative to the off-Bragg intensity) for a symmetric Bragg reflection channel for different values of the phase angle ϕ_h of the unit-cell scattering amplitude. The region $|\eta'| < 1$ corresponds to the Bragg total reflection region. The values of S give the integrated intensities (relative to off Bragg) for the various curves.

$$\mu e^{i\phi_n} = \frac{1}{\nu}\sum_{\rho'} \langle \exp[-i(\vec{k}-\vec{k}_1)\cdot\vec{\rho}']\rangle,$$

$$\doteq \frac{1}{\nu}\sum_{\rho'} \exp\{-\tfrac{1}{2}\langle[(\vec{k}-\vec{k}_1)\cdot(\vec{\rho}'-\vec{R}')]^2\rangle\} \times \exp[-i(\vec{k}-\vec{k}_1)\cdot\vec{R}'], \quad (53)$$

where $\vec{R}' = \langle\vec{\rho}'\rangle$ are the equilibrium positions of the emitters, and where in the second line of (53) we have used the Debye-Waller approximation.

If $\nu > 1$ it is necessary to first obtain the relative positions of the emitting sites together with their Debye-Waller factors so that μ and ϕ_h may be computed; then with these values and our previous expressions modified in accordance with (52) ϕ_h can be determined by Kossel-line analysis. If there are only a small number of emitters per unit cell then their positions should be ascertainable by Mössbauer and/or x-ray-diffraction experiments. If the sources are isotropic $E1$ or $E2$ emitters rather than $M1$, the only change in the previous results is in the interference term. Thus for $E1$ emitters (46) becomes

$$\frac{I_\lambda(\Delta\varphi)}{I_{\lambda 0B}} = 1 - C_\lambda\left(\frac{\sin\varphi_0}{\sin\varphi_1}\right)^{1/2} \times\left(e^{i\phi_h}\left\{\frac{\Delta\varphi'}{w_{\lambda h}} + \left[\left(\frac{\Delta\varphi'}{w_{\lambda h}}\right)^2 - 1\right]^{1/2}\right\}^{-1} + \text{c.c.}\right) + \left(\frac{\sin\varphi_0}{\sin\varphi_1}\right)\left|\frac{\Delta\varphi'}{w_{\lambda h}} + \left[\left(\frac{\Delta\varphi'}{w_{\lambda h}}\right)^2 - 1\right]^{1/2}\right|^{-2}, \quad (54)$$

and $S'_{2\Delta}$ [Eq. (51)] becomes

$$S'_{2\Delta} \doteq \frac{w_{yh}}{2\Delta}\frac{\sin\varphi_0}{\sin\varphi_1} \times\left\{\tfrac{4}{3}(1+\cos\theta) - \tfrac{1}{2}\pi(1+\cos^2\theta)\left(\frac{\sin\varphi_1}{\sin\varphi_0}\right)^{1/2}\sin\phi_h\right\}. \quad (55)$$

And in the case of isotropic $E2$ emitters

$$\frac{I_\lambda(\Delta\varphi)}{I_{\lambda 0B}} = 1 - C'_\lambda\cos\theta\left(\frac{\sin\varphi_0}{\sin\varphi_1}\right)^{1/2} \times\left(e^{i\phi_n}\left\{\frac{\Delta\varphi'}{w_{\lambda h}} + \left[\left(\frac{\Delta\varphi'}{w_{\lambda h}}\right)^2 - 1\right]^{1/2}\right\} + \text{c.c.}\right) + \frac{\sin\varphi_0}{\sin\varphi_1}\left|\frac{\Delta\varphi'}{w_{\lambda h}} + \left[\left(\frac{\Delta\varphi'}{w_{\lambda h}}\right)^2 - 1\right]^{1/2}\right|^{-2} \quad (56)$$

and

$$S'_{2\Delta} = \frac{w_{yh}}{2\Delta}\frac{\sin\varphi_0}{\sin\varphi_1} \times\left\{\tfrac{4}{3}(1+\cos\theta) - \pi\cos^3\theta\left(\frac{\sin\varphi_1}{\sin\varphi_0}\right)^{1/2}\sin\phi_h\right\}. \quad (57)$$

In (56) $C'_x = \cos 2\theta$ and $C'_y = 1$. Comparing these with our previous expressions (46) and (51) it is seen that the major features of the Kossel cones are the same for $E1$ and $E2$ as for $M1$ emitters, there are only minor quantitative differences.

B. Superradiant decay

A point of theoretical interest is the existence of superradiant decay into Bragg modes. That is, an excited nucleus located in a crystal of identical resonant nuclei will decay into the Bragg modes with a radiative width $\Gamma_{\gamma,\mathrm{cr}}$ which is greatly enhanced over the radiative decay width Γ_γ of an isolated nucleus. This of course is closely related to the enhancement of the radiative processes at Bragg discussed in II. This phenomenon was first pointed out by Trammell[16] and Muzikar,[17] and corresponds to Dicke's superradiant emission states.[22]

To illustrate this behavior, we consider a crystal of resonant $M1$ scatterers in their ground state, and an excited source at $\vec{R}_j$. For the "good" $\hat{\epsilon}_x$ polarization, a symmetric channel, and one atom per unit cell, we have $\beta_x = (\delta^2 + 2\delta F_n)^{1/2}$ from (34) and (A3). Since $\beta_x \to 0$ as $\delta \to 0$, the thin-film limit should be used as $\delta \to 0$ even for a thick crystal. We then have

$$\vec{A}'_M(\delta\to 0)\cdot\hat{\epsilon}_x^{(0)} = [\hat{\epsilon}_x^{(0)}\cdot\vec{j}^{f0}(-\vec{k}) + im_j F_n\hat{\epsilon}_x^{(1)}\cdot\vec{j}^{f0}(-\vec{k}_1)] \times e^{-k^2\langle x^2\rangle/2}[\omega - \Delta E + i\tfrac{1}{2}(\Gamma + \Gamma_{\gamma,\mathrm{cr}})]^{-1}, \quad (58)$$

where $\vec{j}(-\vec{k})$ is the Fourier transform of the transition current density as given by Eq. (16) of IIIA, and

$$\Gamma_{\gamma,\mathrm{cr}} = \left(\frac{2\pi M_j \chi^2 n d P(2J_n+1)e^{-k^2\langle x^2\rangle}}{(2J_0+1)\sin\phi_0}\right)\Gamma_\gamma. \quad (59)$$

From (58) we see that the radiative width for decay into the Bragg mode is enhanced by $\Gamma_{\gamma,\mathrm{cr}}$.

As a consequence, the resonance radiation at almost exact Bragg will be frequency broadened, or in time-coincidence experiments, the decay into the Bragg mode occurs more rapidly than isolated decay. This behavior of course only occurs at very near exact Bragg, $\delta \ll 1/M_j$, $1/m_j$. As an example, for Fe^{57} with $m_j = M_j = 10^4$ and $P = \sin\phi_0 = \frac{1}{2}$, then the enhanced width is $\Gamma_{\gamma,\mathrm{cr}} \simeq 6\times 10^2\Gamma_\gamma$, but this behavior occurs only in the extremely narrow collimation $\delta\phi \ll 10^{-5}$ rad (1 sec of arc) about exact Bragg.

It is important to note that these considerations do not contradict the assertion in the Appendix of IIIA that the effective total decay rate Γ' of the atom in the crystal is very nearly equal to the decay rate Γ for an isolated atom, so that it is valid to take $\Gamma' \approx \Gamma$ in Eq. (7) of IIIA for the excited-state propagator G of the nucleus in the crystal. This is because the effective total decay rate in the crystal is determined by the average decay into *all* modes $\vec{k}$, and while there is enhanced decay for $\vec{k}$ *very* near Bragg, there will be a suppression of

decay in other modes, and for most modes the decay rate is essentially unaffected (e.g., off Bragg).

IV. OFF-BRAGG CHANNELS

The most interesting effects in off-Bragg emission are the magneto-optical effects involved in the propagation of the photon through the surrounding medium. In particular, the polarization state of the *recoilless* photon emitted from the crystal will differ from the polarization state at the emitter because of Faraday effects.

Off Bragg only the single $\vec{k}$ channel need be considered. The problem is then formally identical to the off-Bragg external source problem[2,23-25]; therefore we obtain that the coherent wave emitted from the crystal due to a decay at R_j is (Sec. IIB of II)

$$\vec{A}'_M(\vec{k}) = \tilde{D}_j^M(\vec{k}, \vec{k})\vec{J}_\perp(-\vec{k}, \omega; j), \tag{60}$$

where the 2×2 coherent-wave-propagation matrix $\tilde{D}$ is given by

$$\tilde{D}_j^M(\vec{k}, \vec{k}) = \begin{pmatrix} \frac{1}{2}\left[e_{(+)} + e_{(-)}\left(\frac{f_{xx}-f_{yy}}{f_1-f_2}\right)\right] & e_{(-)}\left(\frac{f_{xy}}{f_1-f_2}\right) \\ e_{(-)}\left(\frac{f_{yx}}{f_1-f_2}\right) & \frac{1}{2}\left[e_{(+)} - e_{(-)}\left(\frac{f_{xx}-f_{yy}}{f_1-f_2}\right)\right] \end{pmatrix}, \tag{61}$$

where for $\eta = 1, 2$,

$$f_\eta(\vec{k}, \omega) = \tfrac{1}{2}\,\mathrm{Tr}\tilde{f} + (-1)^{(\eta+1)}\left[\tfrac{1}{4}(\mathrm{Tr}\tilde{f})^2 - \det\tilde{f}\right]^{1/2} \tag{62a}$$

$$= \tfrac{1}{2}(f_{xx}+f_{yy}) + (-1)^{(\eta+1)}\left[\tfrac{1}{4}(f_{xx}-f_{yy})^2 + f_{xy}f_{yx}\right]^{1/2},$$

$$e_{(\pm)}(\vec{k}, \omega; M, R_j) = (e^{if_1 l_j} \pm e^{if_2 l_j})e^{iM_j g_0 d}. \tag{62b}$$

$l_j(\vec{k}) = M_j d/\sin\phi_0$ is the distance the photon travels within the medium in the *direction of emission*, and $f_{ba}(a, b = x \text{ or } y)$ is related to the unit-cell coherent-forward-scattering amplitude for scattering an $|\hat{\epsilon}_a, \vec{k}\rangle$ photon into an $|\hat{\epsilon}_b, \vec{k}\rangle$ photon by

$$f_{ba}(\vec{k}, \omega) = \lambda_0 n \sum_\rho f^{(\rho)}(\hat{\epsilon}_b, \vec{k}; \hat{\epsilon}_a, \vec{k}; \omega), \tag{62c}$$

where n is the unit-cell density, the sum is over the unit cell, and it is understood that the coherent averages are taken at the time of emission, τ_{0j}. Here $\hat{\epsilon}_x$ and $\hat{\epsilon}_y$ can be any orthogonal basis perpendicular to $\vec{k}$.

The photon flux at $\vec{R}$ is then

$$n(\vec{R}, \omega; R_j) = \frac{1}{R^2}\left(\frac{\omega_0}{4\pi^2\hbar c}\right)\mathrm{Tr}\{\tilde{D}_j^M \tilde{n}_0 \tilde{D}_j^{M\dagger}\}, \tag{63}$$

where $\tilde{n}_0$ is the (unnormalized) density matrix for photon emission at R_j,

$$\tilde{n}_0(\vec{k}, \omega; j) = \langle|\vec{J}^{f0}(-\vec{k}, \omega; R_j)\rangle\langle\vec{J}^{f0}(-\vec{k}, \omega; R_j)|\rangle. \tag{64}$$

The expression for $\tilde{n}_0$ for a pure $(L\lambda)$ multipole transition is given by Eq. (A5).

The matrix $\tilde{D}$ describes the propagation of the emitted photon $|J^{f0}(-k, \omega; R_j)\rangle$ through the medium. As discussed in II, and Refs. (23) and (24), for a given frequency ω and direction of propagation $\vec{k}$, there are two eigenwaves $\hat{\epsilon}_\eta(k, \omega)$, $\eta = 1, 2$, which are generally nonorthogonal and have different complex indices of refraction, $n_\eta = 1 + f_\eta$. This leads to Faraday and selective absorption effects, and as a consequence, the polarization state of the *recoilless* photon emitted from the medium will generally differ from the polarization state at the emitter.

The density-matrix formalism gives a convenient description of the polarization state.[26] At the source site the density matrix is

$$\tilde{\rho}_0(\vec{k}, \omega; j) = \frac{\tilde{n}_0}{\mathrm{Tr}\,\tilde{n}_0} = \frac{1}{2}\left(1 + \sum_{i=1}^{3}\xi_i(\vec{k}, \omega)\tilde{\sigma}_i\right). \tag{65a}$$

The polarization state is then described by the Stokes parameters

$$\xi_i(\vec{k}, \omega) = \mathrm{Tr}(\tilde{\rho}_0\tilde{\sigma}_i), \tag{65b}$$

where σ_i, $i = 1, 2, 3$ are the Pauli matrices. In terms of the Stokes parameters the degree of polarization P is

$$P(\vec{k}, \omega) = \left(\sum_{i=1}^{3}\xi_i^2\right)^{1/2}. \tag{65c}$$

External to the crystal, the photon density matrix due to emission at $\vec{R}_j$ is

$$\tilde{\rho}(\vec{k}, \omega; j) = \tilde{D}_j^M \tilde{n}_0 \tilde{D}_j^{M\dagger}/\mathrm{Tr}(\tilde{D}_j^M \tilde{n}_0 \tilde{D}_j^{M\dagger}). \tag{66}$$

The Stokes parameters and degree of polarization at $\vec{R}$ are then given as above.

In general the change of the Stokes parameters

from the source point to the observation point will depend linearly on the concentration of resonant scatterers at the time τ_{0_j}, and upon the propagation distance l_j within the medium.

Such Faraday effects will be strongest for the case of a developed source with moderate Zeeman splitting when there is appreciable overlap between the resonances: In the early development of a source, there is only isotropic electronic scattering within the medium and hence no Faraday effects. For a developed source, in the limit of very strong splitting $g\mu H \gg \Gamma$, a near resonant photon $[\omega \approx \Delta E(M)]$ is almost completely $\vec{Y}^{(\lambda)}_{LM}(\vec{k})$ polarized and in this limit such a photon is an eigenwave of the medium for the given resonant frequency, so that the photon propagated to $\vec{R}$ is also $\vec{Y}^{(\lambda)}_{LM}(\vec{k})$ polarized. In the opposite limit of no Zeeman splitting, the emitted photon is completely unpolarized and any polarization is an eigenwave of the medium, so that the photon at $\vec{R}$ is also completely unpolarized. For these same reasons there are also no Faraday effects for the *recoil fraction*: The emitted recoil fraction emitted from the source is unpolarized, and since the recoil frequencies are nonresonant, the dominant scattering involved is the isotropic electronic scattering so that there are no Faraday effects and the recoil fraction emitted from the crystal is also unpolarized.

V. CRITICAL-ANGLE EMISSION

For γ emission near the critical angle ϕ_c for grazing incidence, the $\vec{k}$ channel and the symmetric $\vec{k}_r$ reflection channel ($\vec{k}_r = -g\hat{z} + \vec{k}_{xy}$) are open, as shown in Fig. 12. Using the development of the last two sections and making the approximations appropriate at grazing incidence as discussed in II, we find that the wave emitted due to a decay at $\vec{R}_j$ is

$$\vec{A}'_M(\vec{k}) = \tilde{D}_c J^{f0}(-\vec{k}, \omega; R_j), \tag{67}$$

where the coherent-wave-propagation matrix $\tilde{D}_c(\vec{k}, \omega; M, \vec{R}_j)$ is given by (61) with $e_{(\pm)}$ replaced by $T_{(\pm)}$,

$$\begin{aligned} T_{(\pm)} &= T_1 \pm T_2, \\ T_\eta &= \exp[ikl_j^\perp(\phi^2 + 2\lambda f_\eta)^{1/2}] \\ &\quad \times \left(\frac{2}{1 + (1 + 2\lambda f_\eta/\phi^2)^{1/2}}\right), \quad \eta = 1, 2 \\ &\equiv \exp[ikl_j^\perp(\phi^2 + 2\lambda f_\eta)^{1/2}] K_\eta, \end{aligned} \tag{68}$$

and f_η is given by (62a). $T_\eta(\vec{k}, \omega; M, \vec{R}_j)$ gives the amplitude for emission of an $\hat{\epsilon}_\eta$ polarized photon from the crystal due to the decay at $\vec{R}_j$, where $\hat{\epsilon}_\eta(\vec{k}, \omega)$, $\eta = 1, 2$, are the two (generally nonorthogonal) eigenwaves. K_η again describes the interference which occurs because two channels are being fed, and the exponential term determines the penetration depth,

$$l_j^\perp = \lambda / \mathrm{Im}(\phi^2 + 2\lambda f_\eta)^{1/2}. \tag{69}$$

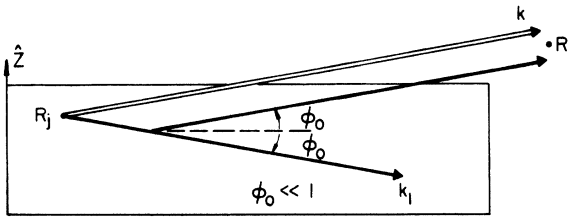

FIG. 12. Schematic representation of a grazing-incidence emission channel.

As for the off-Bragg case, the polarization state of the coherent *resonant* radiation emitted from the crystal will generally differ from the polarization state at the emitter if there is an appreciable fraction of resonant scatterers in the source medium, and if there is Zeeman splitting. The previous development can be taken over directly, and the description of the polarization state is given by formulas (63)–(66) with the replacement of $\tilde{D}_j^M$ by $\tilde{D}_c$.

As shown in Fig. 13(a), the interference term $|K_\eta|^2$ has a maximum $\tilde{<} 4$ at the critical angle $\phi_c = (2\lambda|\mathrm{Re}f_e|)^{1/2}$. The interference is destructive in the total reflection region $\phi < \phi_c$; while for $\phi \gg \phi_c$ there is very little reflection and hence no interference, so that $|K|^2 \to 1$. The penetration depth also has a critical behavior at ϕ_c, rising sharply from strong suppression in the total reflection region $\phi < \phi_c$ to the off-Bragg penetration depth for $\phi > \phi_c$: For $\phi \ll \phi_c$, $l_j^\perp \approx (\lambda/2|\mathrm{Re}f_e|)^{1/2}$, and for example for a pure iron film, emission will only occur from within about 40 Å of the film surface. For $\phi > \phi_c$, the penetration depth rapidly increases to the off-Bragg limit which is $\approx 6\times10^5$ Å for a nonresonant iron film and (for the recoilless fraction) decreases to about 10^4 Å when there is a 10% concentration of resonant scatterers. In the region within the interference bright spot $\phi \tilde{>} \phi_c$, the penetration depth is rapidly increasing and, for example, for a nonresonant iron film at $\phi = 4.0\times10^{-3}$ rad, $l_j^\perp \approx 750$ Å; while for $\phi = 6.2\times10^{-3}$ rad, $l_j^\perp \approx 3\times10^3$ Å.

Although there is an interference bright spot near the critical angle, the maximum intensity for a *given collimation* from a *thick* film in the grazing incidence direction is less than the maximum intensity in the direction normal to the film if the sources are uniformly distributed to the off-Bragg penetration depth l_{0B}. In Fig. 13(b) we show the ratio of the intensity obtained in the normal direction from a thick film of surface area l^2 to that obtained at grazing incidence from a film of surface area (l^2/ϕ). Within the critical reflection region the

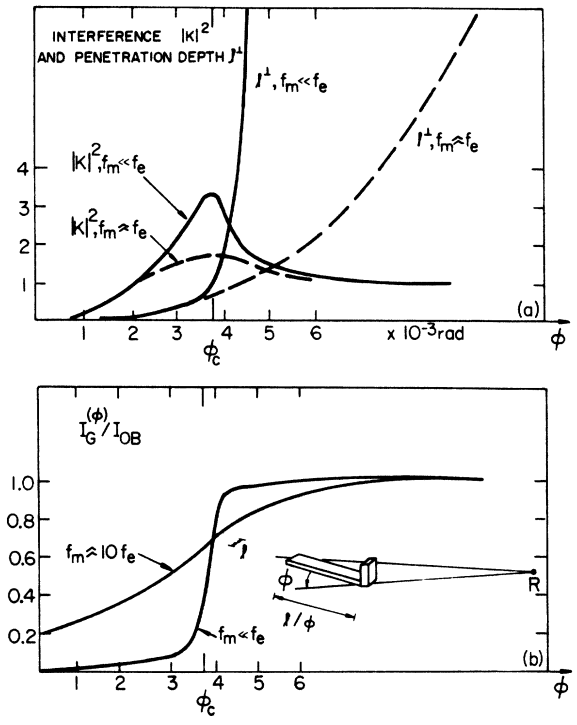

FIG. 13. (a) Plots of the interference term $|K|^2$ and the penetration depth $l^\perp$ vs the rocking angle ϕ for Fe^{57} in Fe. The solid curves ($f_n \ll f_e$) are for the early development, and the dashed curves ($f_n \approx f_e$) are for the recoilless fraction in a developed source. $\phi_c \approx 3.8 \times 10^{-3}$ rad is the critical angle for total reflection. (b) Plots of the intensity emitted at the grazing angle ϕ from a film with a uniform distribution of emitters relative to the intensity obtained off Bragg from a thick crystal uniformly populated with the same fraction of emitters.

relative intensity at grazing incidence is $\ll 1$ due to the shallow penetration depth and the destructive interference in this region. Within a narrow region $\phi \gtrsim \phi_c$, however, there is a very rapid increase in the relative intensity although the penetration depth is still relatively shallow. As a practical matter, some advantage can be obtained from this behavior in preparing collimated sources. For example, if Co^{57} is spread over a film surface of ($l \times 250l$) to a depth of 750 Å, the source will have a bright spot 2.3 times background at $\varphi = 4 \times 10^{-3}$ rad which will be 73% as intense as a normally oriented *thick* source of surface area l^2, which contains the same density of Co^{57} to the off-Bragg penetration depth of 6×10^5 Å. Although the intensity is down by 27%, only surface deposition is required and only $\frac{1}{3}$ as much source material is required.

VI. SUMMARY

The purpose of this paper has been to present a comprehensive investigation of the emission of Mössbauer γ rays from single crystals, and to examine in particular the emission into Laue, Bragg, off-Bragg, and grazing-incidence channels.

Initially our primary motivation in this investigation was to see if coherence effects in the emission from single crystals could lead to enhanced collimated sources of radiation. Our conclusion on this point is that a limited short-lived enhancement can be achieved in the highly collimated Laue channels during the early development of an active source of multipolarity $M1$ or higher due to the "anomalous-emission" effect. However, quite aside from the question of enhanced sources, and of potentially greater importance, the Kossel pattern itself is of considerable interest. In particular, the Bragg or Laue channel "magnetic Kossel lines," which are a feature unique to the Mössbauer case, offer a sensitive probe of the magnetic (or electric-field-gradient) structure and its dependence on temperature and strain. In addition, accurate intensity measurements of the Kossel lines will give phase information about the unit-cell scattering amplitude. For off-Bragg or grazing-incidence emission, the most interesting aspect is the Faraday effects which occur for the Mössbauer case. Also grazing-incidence emission offers some practical advantages for producing intense collimated sources.

ACKNOWLEDGMENTS

We would like to acknowledge useful conversations with R. L. Mössbauer and F. Parak during the early stages of this work.

APPENDIX

For reference, we summarize here some useful multipole formulas.

For a pure ($LM\lambda$) multipole transition from an excited Zeeman level ($J_m m_m$) to a ground state (J_0, m_0), the transverse component of the source current Eq. (15) of IIIA is given by

$$\vec{J}^{f0}(-\vec{k},\ \omega;\ l) = c^{-1}\langle \chi_f | e^{-i\vec{k}\cdot\vec{r}_l} | \chi_0 \rangle \times [\omega + E(J_0 m_0) + \epsilon_f - E(J_n m_n) - \epsilon_0 + i\Gamma/2]^{-1} \times C(J_0 L J_n;\ m_0 M m_n)[\lambda_0 \Gamma_\gamma(L\lambda)]^{1/2}\, \vec{Y}_{LM}^{(\lambda)}(\hat{k}), \qquad \text{(A1)}$$

where $C(J_0 L J_m;\ m_0 M m_m)$ is the Clebsch-Gordan coefficient for the transition, $\Gamma_\gamma(L\lambda)$ is the radiative width associated with the emission of (L, λ) multipole radiation, and $\vec{Y}_{LM}^{(\lambda)}$ is a vector spherical harmonic. For an $E1$ transition ($L = 1$, $\lambda = 1$), the spherical harmonics are given explicitly by

$$\vec{Y}_{10}^{(1)}(\hat{k}) = -(3/8\pi)^{1/2} \sin\theta \hat{e}_\theta, \qquad \vec{Y}_{1\pm1}^{(1)}(\hat{k}) = (3/16\pi)^{1/2} e^{\pm i\phi}[\mp \cos\theta \hat{e}_\theta - i\hat{e}_\phi]. \qquad \text{(A2)}$$

Here $\hat{e}_\theta$ and $\hat{e}_\phi$ are the usual spherical polar unit vectors, and θ and ϕ are the polar and axial angles

specifying the emission direction $\vec{k}$, with the $\hat{z}$ axis coinciding with the quantization axis at the nucleus. For an $M1$ transition ($L=1$, $\lambda=0$) the spherical harmonics are

$$\vec{Y}_{10}^{(0)}(\hat{k}) = i(3/8\pi)^{1/2}\sin\theta\hat{e}_\phi\,,$$
$$\vec{Y}_{1\pm1}^{(0)}(\hat{k}) = (3/16\pi)^{1/2}e^{\pm i\phi}(\hat{e}_\theta \pm i\cos\theta\hat{e}_\phi)\,, \qquad (A2')$$

and for an $E2$ transition ($L=2$, $\lambda=1$),

$$\vec{Y}_{20}^{(1)}(\hat{k}) = -(15/32\pi)^{1/2}\sin(2\theta)\hat{e}_\theta\,,$$
$$\vec{Y}_{2\pm1}^{(1)}(\hat{k}) = (5/16\pi)^{1/2}e^{\pm i\phi} \times[\mp\cos(2\theta)\hat{e}_\theta - i\cos\theta\hat{e}_\phi]\,, \qquad (A2'')$$
$$\vec{Y}_{2\pm2}^{(1)}(\hat{k}) = (5/16\pi)^{1/2}e^{\pm i2\phi} \times[\tfrac{1}{2}\sin(2\theta)\hat{e}_\theta \pm i\sin\theta\hat{e}_\phi]\,.$$

The planar scattering amplitude $F_{\lambda\lambda'}^{\tau\tau'}$ entering into the multiple-scattering equations (58) of IIIA is related to the atomic coherent elastic scattering amplitude $f_{\eta\eta'}^{\tau\tau'} = f(\hat{\epsilon}_\eta(\vec{k}_\tau), \vec{k}_\tau; \hat{\epsilon}_{\eta'}(k_{\tau'}), k_{\tau'}; \omega)$ by Eq. (7). The general multipole expansion for the resonant nuclear scattering contribution to $f_{\eta\eta'}^{\tau\tau'}$ is given by Eq. (4) of II. In the limit of no Zeeman splitting, for a pure $L\lambda$ multipole transition, the nuclear contribution becomes

$$f_{\eta\eta}^{\tau\tau'} = \tfrac{1}{2}\lambda_0 e^{-k^2\langle x^2\rangle}\left(\frac{2J_n+1}{2J_0+1}\right)\left(\frac{\Gamma_\gamma}{\Gamma}\right)\frac{C_{\eta\eta}^{\tau\tau'}(\theta)}{x(d_n,d_0)-i}\,. \qquad (A3)$$

Here $x = 2[E(J_n) - E(J_0) - \hbar\omega]/\Gamma$ is the deviation of the photon frequency from exact resonance in units of the half-width, $\eta = x$ or y refers to the *linear* basis vectors $\hat{\epsilon}_x^{(\tau)}$, $\hat{\epsilon}_y^{(\tau)}$ discussed in Sec. II, and

TABLE II. Tabulation of the angular function $C_{\eta\eta}^{\tau\tau'}(\theta)$ for the $E1$, $M1$, and $E2$ multipole cases.

	$C_{xx}^{tt} = C_{yy}^{tt}$	$C_{yy}^{t_0t_1}$	$C_{xx}^{t_0t_1}$
$E1$	1	1	$\cos\theta$
$M1$	1	$\cos\theta$	1
$E2$	1	$\cos\theta$	$\cos2\theta$

$C_{\eta\eta}^{\tau\tau'}(\theta)$ is a function of the scattering angle θ between $k_{\tau'}$ and k_τ which depends upon the multipolarity of the transition. In Table II we tabulate $C_{\eta\eta}^{\tau\tau'}$ for the $E1$, $M1$, and $E2$ multipole cases. For all cases the total absorption cross section is given by

$$\sigma_n = \frac{4\pi}{k}\,\mathrm{Im}\,f_{\eta\eta}^{\tau\tau} = 2\pi\lambda^2 e^{-k^2\langle x^2\rangle}\left(\frac{2J_n+1}{2J_0+1}\right)\left(\frac{\Gamma_\gamma}{\Gamma}\right)\left(\frac{1}{x^2+1}\right). \qquad (A4)$$

The electronic contribution to the coherent elastic scattering amplitude is

$$f_{\eta\eta}^{\tau\tau'} = \hat{\epsilon}_\eta^{(\tau)}\cdot\hat{\epsilon}_\eta^{(\tau')} f_D(\theta)[-r_0F(\theta) + i(k_0/4\pi)\sigma_{pe}]\,, \qquad (A5)$$

where $\eta = x$ or y again refers to the linear $\hat{\epsilon}_x$, $\hat{\epsilon}_y$ bases, $f_D(\theta) = \exp(-\frac{1}{2}\langle[(\vec{k}_\tau - \vec{k}_{\tau'})\cdot x]^2\rangle)$ is the Debye phonon factor, $r_0 = e^2/mc^2$, $F(\theta) = \langle e_0|\sum_i e^{i(k_\tau - k_{\tau'})\cdot\vec{x}_i}|e_0\rangle$ is the electronic form factor, and σ_{pe} is the photoelectric cross section.

Finally, the (unnormalized) density matrix (64) for the *recoilless* emission of a $|\vec{k}, \omega\rangle$ photon from a pure ($L\lambda$) multipole transition for which $J_z = m$ is a good quantum number is given by

$$\tilde{n}_0(\vec{k},\omega) = K\sum_{m=-L}^{+L}\sum_{m_n}\frac{P(m_n)C^2(J_0LJ_n;\, m_0Mm_n)}{[\omega - E(J_nm_n) + E(J_0m_0)]^2 + \Gamma^2/4} \times\begin{pmatrix} [d_{1M}^{(L)}(\theta)]^2 & (-1)^{(\lambda+1)}d_{1M}^{(L)}(\theta)d_{-1M}^{(L)}(\theta) \\ (-1)^{(\lambda+1)}d_{1M}^{(L)}(\theta)d_{-1M}^{(L)}(\theta) & [d_{-1M}^{(L)}(\theta)]^2 \end{pmatrix}. \qquad (A6)$$

Here $P(m_n)$ is the probability that initially the nucleus is in the excited state $|J_nm_n\rangle$, θ is the polar angle from the quantization axis $\hat{z}$ to $\hat{k}$, the notation for the rotation matrices $d_{\mu M}^{(L)}(\theta)$ is that of Rose,[27] and the constant

$$K = c^{-2}e^{-k^2\langle x^2\rangle}\lambda_0\Gamma_\gamma\left(\frac{2L+1}{8\pi}\right).$$

*Work supported in part by the National Science Foundation. Early stages of work supported in part by the Office of Naval Research under Contract No. N00014-68-A-0503.

†Present address: Mission Research Corp., P. O. Drawer 719, Santa Barbara, Calif. 93102.

[1]J. P. Hannon, N. J. Carron, and G. T. Trammell, preceeding paper, Phys. Rev. B 9, 2791 (1974). We will refer to this paper as IIIA.

[2]J. P. Hannon and G. T. Trammell, Phys. Rev. 186, 306 (1969). We will refer to this paper as II.

[3]V. A. Belyakov, Fiz. Tverd. Tela 13, 2170 (1971) [Sov. Phys.-Solid State 13, 1824 (1972)].

[4]G. Borrmann, Z. Phys. 42, 157 (1941). For a discussion of the x-ray Borrmann effect see Refs. 5 and 6, and also P. P. Ewald, Rev. Mod. Phys. 37, 46 (1965).

[5]Max von Laue, *Rontgenstrahleninterferenzen* (Akademische Verlagsgesellschaft, Frankfurt am Main,

1960), pp. 430–448.
[6]R. W. James, *The Optical Principles of the Diffraction of X Rays* (Cornell U. P., Ithaca, N. Y., 1965), pp. 413–457.
[7]J. P. Hannon and G. T. Trammell, Phys. Rev. 169, 315 (1968). This paper will be referred to as I.
[8]P. J. Black, Nature 206, 1223 (1965).
[9]F. Parak, R. L. Mössbauer, U. Biebl, H. Formanek, and W. Hoppe, Z. Phys. 244, 456 (1971).
[10]An alternate and experimentally much simpler method of separation is to reflect the initial x-ray–γ-ray beam from any single crystal with the orientation chosen such that the 13.5-keV γ ray will be Bragg reflected. The Bragg-reflected beam will then be an almost pure γ-ray source.
[11]P. A. Alexandrov and Yu. Kagan, Zh. Eksp. Teor. Fiz. 59, 1733 (1970) [Sov. Phys.-JETP 32, 942 (1972)].
[12]G. T. Trammell, paper presented to the Budapest Mössbauer Conference, May, 1969 (unpublished). An investigation of this effect was carried out by F. von Erdman, Ph. D. thesis (Technische Hochschule München, 1970) (unpublished).
[13]R. E. DeWames and W. F. Hall, Acta Crystallogr. A 24, 206 (1968).
[14]B. W. Batterman, Phys. Rev. Lett. 22, 703 (1969).
[15]See, for example, R. Tixier and C. Wache, J. Appl. Crystallogr. 466 (1970).
[16]G. T. Trammell, *Chemical Effects on Nuclear Transformations* (International Atomic Energy Agency, Vienna, 1961), Vol. I, p. 75.
[17]C. Muzikar, Zh. Eksp. Teor. Fiz. 41, 1168 (1961).
[18]D. F. Zaretskii and V. V. Lomonosov, Zh. Eksp. Teor. Fiz. 48, 368 (1965) [Sov. Phys.-JETP 21, 243 (1965)].
[19]A. M. Afanas'ev and Yu. Kagan, Zh. Eksp. Teor. Fiz. 48, 327 (1965) [Sov. Phys.-JETP 21, 215 (1965)].
[20]Max von Laue, Ann. Phys. 31, 705 (1935).
[21]For a discussion of the crystalline properties of myoglobin see G. Bodo, H. M. Dintra, V. C. Kendrew, and H. W. Wyokoff, Proc. R. Soc. A 253, 70 (1959); or F. Parak, Ph. D. thesis, (Technische Hochschule München, 1970) (unpublished).
[22]R. H. Dicke, Phys. Rev. 93, 99 (1954).
[23]M. Blume and O. C. Kistner, Phys. Rev. 171, 417 (1968).
[24]R. M. Housley, R. W. Grant, and V. Gonser, Phys. Rev. 178, 514 (1969).
[25]J. P. Hannon, Nucl. Phys. A 177, 493 (1971).
[26]See for example A. I. Akhiezer and V. B. Berestetskii, *Quantum Electrodynamics* (Wiley-Interscience, New York, 1965), pp. 13–17.
[27]M. E. Rose, *Elementary Theory of Angular Momentum* (Wiley, New York, 1957), pp. 32–48.